

Removal and Binding Energies in Lepton Nucleus Scattering

A. Bodek

Department of Physics and Astronomy, University of Rochester, Rochester, NY 14627-0171

Received: date / Revised version: July 8, 2018

Abstract. We investigate the binding energy parameters that should be used in modeling electron and neutrino scattering from nucleons bound in a nucleus within the framework of the impulse approximation. We discuss the relation between binding energy, removal energy, interaction energy, spectral functions and shell model energy levels and extract updated interaction energy parameters from modern $ee'p$ spectral function data. We address the difference in parameters for scattering from bound protons and neutrons, and the difference between the parameters for modeling the *peak* (most probable value) versus the *mean* of distributions. We show that different MC generators use different definitions of what is referred to as nuclear interaction energy parameters. For example, for neutrino scattering from neutrons bound in $^{16}_8\text{O}$ the Smith-Moniz interaction energy $\langle \epsilon_{SM}^N \rangle = 43.0 \pm 3$ MeV should be used in NEUT, the excitation energy $\langle E_x^N \rangle = 10.2 \pm 3$ MeV should be used in GENIE, and the interaction energy $\langle \epsilon_R^N \rangle = 27.0 \pm 3$ should be used to calculate the neutrino energy from muon variables only. At present the uncertainty in the value of the interaction energy (± 15 MeV) results in the largest systematic uncertainty (± 0.033 eV^2) in the extraction of the neutrino oscillation parameter Δm^2 . We reduce this uncertainty by a factor of 5.

PACS. 13.60.Hb Total and inclusive cross sections (including deep-inelastic processes) – 13.15.+g Neutrino interactions – 13.60.-r Photon and charged-lepton interactions with hadrons

1 Introduction

The modeling of neutrino cross sections on nuclear targets is of great interest to neutrino oscillations experiments. Neutrino Monte Carlo (MC) generators include GENIE[1], NEUGEN[2], NEUT[3], NUANCE[4], NUWRO[5] and GiBUU[6].

Although more sophisticated models are available[7–9], calculations using a one-dimensional momentum distribution and an average binding energy parameter are still widely used. One example is the simple relativistic Fermi gas (RFG) model.

The RFG model does not describe the tails in the energy distribution of the final state lepton very well[10,11]. Improvements to the RFG model such as a better momentum distribution are usually made within the existing Monte Carlo (MC) frameworks. All RFG-like models with different nucleon momentum distributions require in addition an average binding energy parameter (interaction energy) to account for the removal energy of nucleons from the nucleus. The interaction energy should be the same for all one-dimensional momentum distributions. In more sophisticated impulse approximation models[7–9] two dimensional spectral functions (as a function of nucleon momentum and removal energy) are used.

1.1 Relevance to neutrino oscillations experiments

In a two neutrinos oscillations framework the oscillation parameters which are extracted from long baseline experiments are the mixing angle ϑ and the square of the difference in mass between the two neutrino mass eigenstates Δm^2 . A correct modeling of the reconstructed neutrino energy is very important in the measurement of Δm^2 . In general, the resolution in the measurement of energy in neutrino experiments is much worse than the resolution in electron scattering experiments. However, a precise determination of Δm^2 is possible if the MC prediction for *mean* value of the experimentally reconstructed neutrino energy is unbiased. At present the uncertainty in the value of the interaction energy is a significant source of systematic error in the extraction of the neutrino oscillation parameter Δm^2 (as shown below).

The two-neutrino transition probability can be written as

$$P_{\nu_\alpha \rightarrow \nu_\beta}(L) = \sin^2 2\vartheta \sin^2 \left(1.27 \frac{(\Delta m^2 / \text{eV}^2) (L / \text{km})}{(E_\nu / \text{GeV})} \right). \quad (1)$$

Here, L (in km) is the distance between the neutrino source and the detector and Δm^2 is in eV^2 .

The location of the first oscillation maximum in neutrino energy ($E_\nu^{1st-min}$) is when the term in brackets is equal to $\pi/2$. An estimate of the extracted value of Δm^2

is given by:

$$\Delta m^2 = \frac{2E_\nu^{1st-min}}{1.27\pi L}. \quad (2)$$

For example, for the T2K experiment[12] $L = 295 \text{ Km}$, and E_ν is peaked around 0.6 GeV . The T2K experiment[12] reports a value of

$$\Delta m_{32}^2 = (2.434 \pm 0.064) \times 10^{-3} \text{ eV}^2.$$

In the Monte Carlo generator used by T2K (NEUT) a value of the interaction energy of 27 MeV for ${}^{16}_8\text{O}$ has been used. However, as we show in section 7 a value of 43 MeV should be used. Using equation 2 in conjunction with equation 40 of Appendix D we estimate that a $+15 \text{ MeV}$ change in $\langle \epsilon'_{SM} \rangle$ results in a change in Δm_{32}^2 of $+0.033 \times 10^{-3} \text{ eV}^2$, which is the largest contribution to the total systematic error in Δm_{32}^2 . As we show in this communication, this contribution can be reduced by a factor of 5.

For comparison, a change of $+15 \text{ MeV}/c$ in the assumed value of the Fermi momentum K_F yields a smaller change of $+0.003 \times 10^{-3} \text{ eV}^2$ in the extracted value of Δm_{32}^2 .

1.2 Nucleon momentum distributions

Fig. 1 shows a few models for the nucleon momentum distributions in the ${}^{12}_6\text{C}$ nucleus. The solid green line (labeled Global Fermi gas) is the nucleon momentum distribution for the Fermi gas[10] which is currently implemented in all neutrino event generators and is related to global average density of nucleons. The solid black line is the projected momentum distribution of the Benhar-Fantoni[7] 2D spectral function as implemented in NUWRO. The solid red line is the nucleon momentum distribution for the Local-Thomas-Fermi (LTF) gas which is related to the local density of nucleons in the nucleus and is implemented in NEUT, NUWRO and GIBUU.

For QE scattering, another more sophisticated formalism is the ψ' superscaling model[13] discussed in Appendix E. This model is only valid for QE scattering. It can be used to predict the kinematic distribution of the final state muon but does not describe the details of the hadronic final state. Therefore, it has not been implemented in neutrino MC generators. However, the predictions of the ψ' superscaling model can be approximated with an effective spectral function[8] which has been implemented in GENIE. The momentum distribution of the effective spectral function for nucleons bound in ${}^{12}_6\text{C}$ is shown as the blue curve in Fig. 1.

Although the nucleon momentum distributions are very different for the various model, the predictions for the normalized quasielastic neutrino cross section $\frac{1}{\sigma} \frac{d\sigma}{d\nu}(Q^2, \nu)$ are similar as shown in Fig. 2. These predictions as a function of $\nu = E_\nu - E_\mu$ are calculated for 10 GeV neutrinos on ${}^{12}_6\text{C}$ at $Q^2=0.5 \text{ GeV}^2$. The prediction with the local Fermi gas distribution are similar to the prediction of the Benhar-Fantoni two dimensional spectral function as implemented in NUWRO. Note that the prediction of the ψ'

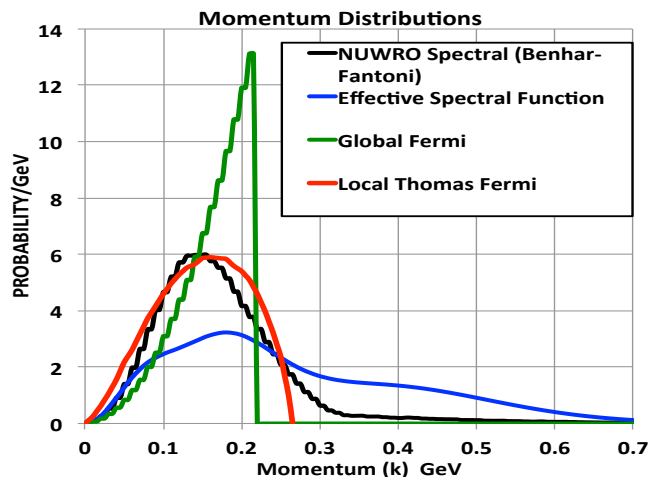


Fig. 1. One-dimensional nucleon momentum distributions in a ${}^{12}_6\text{C}$ nucleus. The green curve (Global Fermi) is the momentum distribution for the relativistic Fermi gas (RFG) model which is related to global average density of nucleons. The red curve is the local Fermi gas distribution which is related to the local density of nucleons in the nucleus. The black curve is the projected momentum distribution of the Benhar-Fantoni two dimensional spectral function as implemented in NUWRO. The blue line is the momentum distribution for the *effective spectral function* model, which approximates the ψ' superscaling prediction for the final state muon in quasielastic scattering. The *effective spectral function* is only valid for QE scattering because the ψ' superscaling model is only valid for QE scattering.

superscaling model are based on fits to electron QE scattering data and therefore includes both the $1p1h$ and $2p2h$ processes (discussed in section 3).

The following nuclear targets are (or were) used in neutrino experiments: Carbon (scintillator) used in the NOVA and MINER ν A experiments. Oxygen (water) used in T2K, and in MINER ν A. Argon used in the ARGONEUT and DUNE experiments. Calcium (marble) used in CHARM. Iron used in MINER ν A, MINOS, CDHS, NUTEV, and CCFR. Lead used in CHORUS and MINER ν A.

2 Deficiencies in current MC generators

Deficiencies in the current implementations in neutrino MC generators originate from several sources.

1. Using the published values of parameters extracted by Moniz et. al.[10] and not correcting for the approximations used in that analysis.
2. Using the same values of the interaction energy in different MC generators not accounting for the fact that they are defined differently in each generator.
3. Not accounting for nuclear Coulomb corrections[14] to the energies of charged leptons in the initial and final state.
4. The interaction energies extracted by Moniz et. al. from high resolution electron scattering experiments

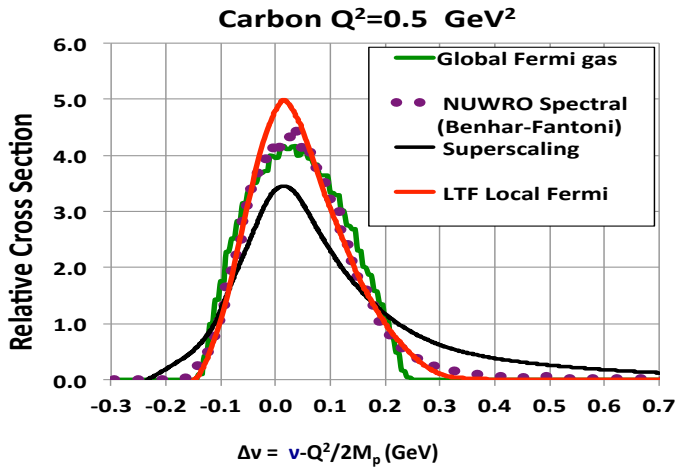


Fig. 2. Comparison of the ψ' superscaling prediction (solid black line) for the normalized quasielastic $\frac{1}{\sigma} \frac{d\sigma}{d\nu}(Q^2, \nu)$ at $Q^2=0.5 \text{ GeV}^2$ for 10 GeV neutrinos on ^{12}C to the predictions with several momentum distribution ($\nu = E_\nu - E_\mu$). Here the solid green curve labeled "Global Fermi" gas is the distribution for the Fermi gas model. The red line is the prediction for the local Thomas Fermi (LTF) gas, and the purple dots are the prediction using the two dimensional Benhar-Fantoni spectral function as implemented in NUWRO.

typically reflect the $[peak]$ (most probable value) of the distribution of the energy of the final state electron for QE scattering events. In contrast, the parameters for neutrino experiments should be chosen to correctly model the $\langle mean \rangle$ reconstructed final state lepton energy of QE events. The interaction energy parameters for modeling the $\langle mean \rangle$ are larger.

In this paper we primarily focus on extracting values for the interaction energies from more recent $ee'p$ electron scattering data. We use experimental measurements whenever possible and only used theoretical input when necessary (e.g. relating neutron to proton parameters). Consequently, we reduce the overall systematic uncertainty in the removal energy parameters from $\pm 15 \text{ MeV}$ to $\pm 3 \text{ MeV}$.

In general we use square brackets to denote the $[peak]$ position and angular brackets to denote the $\langle mean \rangle$ value. We consistently use units of MeV for nuclear binding energy, interaction energy, removal energy, and excitation energy. We use units of MeV/c for Fermi momenta.

We can extract interaction and removal energy parameters from electron scattering data from a variety of modern experiments in three different ways.

1. The $mean$ removal energy extracted for tests of the Kotlun[15] sum rule from $ee'p$ spectral functions.
2. The $mean$ removal energy extracted from the weighted average of the removal energies of shell-model energy levels as measured in $ee'p$ experiments.
3. The location of the QE $peak$ in inclusive e-A scattering (e.g. Moniz et. al.) with additional corrections described below.

In our summary tables, for each nucleus we select a single measurement which we consider to be the most reliable.

As discussed in section 6, method 1 is the most reliable, followed by method 2. Here, method 3 is only used as a consistency check.

2.1 Corrections to the Moniz et. al. analysis

The interaction energies published by Moniz et. al. in 1971 (method 3) were extracted within the framework of the RFG model *without* accounting for acceleration or deceleration in the Coulomb field of the nucleus[14] (Coulomb corrections). In addition, energy conserving relativistic kinematics were not used. Therefore, corrections for these deficiencies must be applied in order to be able to use these results for consistency checks.

We first apply Coulomb and relativistic corrections to the Moniz analysis and re-extract updated values of interaction energies and Fermi momenta. We discuss the relation between binding energy, removal energy, interaction energy, spectral functions and shell model energy levels, and the difference for scattering from bound protons and neutrons. We discuss how to account for the violation of energy conservation in the Moniz et. al.[10] and the Smith-Moniz[11] implementations formalism. And finally we show that as a consistency check, these updated values are consistent with more reliable parameters that we extract from $ee'p$ spectral function measurements

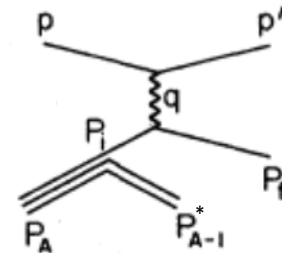


Fig. 3. 1p1h process: Scattering from an off-shell bound proton of momentum $\mathbf{p}_i=\mathbf{k}$ in a nucleus of mass A. Here, the nucleon is moving in the mean field (MF) of all other nucleons in the nucleus. The on-shell recoil excited $[A-1]^*$ spectator nucleus has a momentum $\mathbf{p}_{(A-1)^*} = -\mathbf{k}$. The off-shell energy of the interacting nucleon is $E_i = M_A - \sqrt{(M_{A-1})^2 + \mathbf{k}^2} = M_A - \sqrt{(M_{A-1} + E_x)^2 + \mathbf{k}^2}$, where E_x is the excitation energy of the $[A-1]^*$ spectator nucleus.

3 The Impulse Approximation

3.1 1p1h process

Fig. 3 is a descriptive diagram for QE lepton (electron, muon or neutrino) scattering on an off-shell nucleon which is bound in a nucleus of mass M_A . Here, the nucleon is moving in the mean field (MF) of all other nucleons in the nucleus. For example, for *electron scattering* on

$\frac{A}{Z}Nucl$	remove proton Spectator	S^P	remove neutron Spectator	S^N	S^{N+P}
${}^2_1\text{H}$	N	2.2	P	2.2	2.2
${}^6_3\text{Li } 1+$	${}^5_2\text{He } \frac{3}{2}-$	4.4	${}^5_3\text{Li } \frac{3}{2}-$	5.7	4.0
${}^{12}_6\text{C } 0+$	${}^{11}_5\text{B } \frac{3}{2}-$	16.0	${}^{11}_6\text{C } \frac{3}{2}-$	18.7	27.4
${}^{16}_8\text{O } 0+$	${}^{15}_7\text{N } \frac{1}{2}-$	12.1	${}^{15}_8\text{O } \frac{1}{2}-$	15.7	23.0
${}^{24}_{12}\text{Mg } 0+$	${}^{23}_{11}\text{Na } \frac{3}{2}+$	11.7	${}^{23}_{12}\text{Mg } \frac{3}{2}+$	16.5	24.1
${}^{27}_{13}\text{Al } \frac{5}{2}+$	${}^{26}_{12}\text{Mg } 0+$	8.3	${}^{26}_{13}\text{Al } 5+$	13.1	19.4
${}^{28}_{14}\text{Si } 0+$	${}^{27}_{13}\text{Al } \frac{5}{2}+$	11.6	${}^{27}_{14}\text{Si } \frac{5}{2}+$	17.2	24.7
${}^{40}_{18}\text{Ar } \frac{3}{2}+$	${}^{39}_{17}\text{Cl } \frac{3}{2}+$	12.5	${}^{39}_{18}\text{Ar } \frac{7}{2}-$	9.9	20.6
${}^{40}_{20}\text{Ca } 0+$	${}^{39}_{19}\text{K } \frac{3}{2}+$	8.3	${}^{39}_{20}\text{Ca } \frac{3}{2}+$	15.6	21.4
${}^{51}_{23}\text{V } \frac{7}{2}-$	${}^{50}_{22}\text{Ti } 0+$	8.1	${}^{50}_{23}\text{V } 6+$	11.1	19.0
${}^{56}_{26}\text{Fe } 0+$	${}^{55}_{25}\text{Mn } \frac{5}{2}-$	10.2	${}^{55}_{26}\text{Fe } \frac{3}{2}-$	11.2	20.4
${}^{58}_{28}\text{Ni } \frac{3}{2}-$	${}^{58}_{27}\text{Co } 2+$	8.2	${}^{58}_{28}\text{Ni } 0+$	12.2	19.5
${}^{89}_{39}\text{Y } \frac{1}{2}-$	${}^{88}_{38}\text{Sr } \frac{1}{2}-$	7.1	${}^{88}_{39}\text{Y } 4-$	11.5	18.2
${}^{90}_{40}\text{Zr } 0+$	${}^{89}_{39}\text{Y } \frac{1}{2}-$	8.4	${}^{90}_{40}\text{Zr } \frac{9}{2}+$	12.0	17.8
${}^{120}_{50}\text{Sn } 0+$	${}^{119}_{49}\text{In } \frac{9}{2}+$	10.1	${}^{119}_{50}\text{Sn } \frac{1}{2}+$	8.5	17.3
${}^{181}_{73}\text{Ta } \frac{7}{2}-$	${}^{180}_{72}\text{Hf } 0+$	5.9	${}^{180}_{73}\text{Ta } 1+$	7.6	13.5
${}^{197}_{79}\text{Au } \frac{3}{2}+$	${}^{196}_{78}\text{Pt } 0+$	5.8	${}^{196}_{79}\text{Au } 2-$	8.1	13.7
${}^{208}_{82}\text{Pb } 0+$	${}^{207}_{81}\text{Tl } \frac{1}{2}+$	8.0	${}^{207}_{82}\text{Pb } \frac{1}{2}-$	7.4	14.9

Table 1. The spin parity transitions and separation energies S^P , S^N and S^{N+P} when a proton or a neutron or both are removed from various nuclei. All energies are in MeV.

a off-shell bound proton of momentum $\mathbf{p}_i=\mathbf{k}$, the recoil $[A-1]^*$ (spectator) nucleus is on-shell and has momentum $\mathbf{p}_{(A-1)^*} = -\mathbf{k}$. The * is used to indicate that the spectator nucleus is not necessarily in the ground state. This process is referred to as the 1p1h process (one proton and one hole). Table 1 shows the spin and parity of the initial state nucleus, and the spin parity of the ground state of the spectator nucleus when a bound proton or a bound neutron is removed via the 1p1h process.

The four-momentum transfer to the nuclear target is defined as $q = (\mathbf{q}, \nu)$. Here \mathbf{q} is the 3-momentum transfer, ν is the energy transfer, and $Q^2 = -q^2 = \nu^2 - \mathbf{q}^2$ is the square of the four-momentum transfer. For QE electron scattering on unbound protons (or neutrons) the energy transfer ν is equal to $Q^2/2M_{p,n}$ where M_p is mass of the proton and M_n is the mass of the neutron, respectively.

3.2 Two nucleon correlations

Fig. 4 illustrates the 2p2h process originating from short range two nucleon correlations (SRC). Here the scattering is from an off-shell bound proton of momentum $\mathbf{p}_i=\mathbf{k}$. The momentum of the initial state off-shell interacting nucleon is balanced by a single on-shell correlated recoil neutron which has momentum $-\mathbf{k}$. The $[A-2]^*$ spectator nucleus is left with two holes. Short range nucleon-proton correlations occur $\approx 20\%$ of the time[16]. As discussed in section 4.7. The off-shell energy of the interacting bound proton in a quasi-deuteron is $(E_i^P)_{SRC} = M_D - \sqrt{M_n + \mathbf{k}^2} - \Delta_{SRC}^{N+P}$, where Δ_{SRC}^{N+P} is the removal energy of the two nucleons and M_D is the mass of the deuteron, For QE scattering there

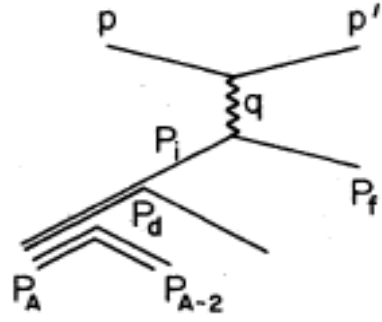


Fig. 4. 2p2h process: Scattering from an off-shell bound proton of momentum $\mathbf{p}_i=\mathbf{k}$ from two nucleon short range correlations (quasi-deuteron). There is an on-shell spectator $(A-2)^*$ nucleus and an on-shell spectator recoil neutron with momentum $-\mathbf{k}$. The off-shell energy of the interacting bound proton is $E_i^P(SRC) = M_D - \sqrt{M_n + \mathbf{k}^2} - \Delta_{SRC}^{N+P}$.

is an additional 2p2h transverse cross section from "Meson Exchange Currents" (MEC) and "Isobar Excitation" (IE).

In this paper we only focus the extraction the *mean* interaction energy parameters for 1p1h processes. Processes leading to 2p2h final states (SRC, MEC and IE) result in larger removal energy and should be modeled separately.

4 Energy-Momentum Conservation

For QE electron scattering the energy-momentum δ function and the final state nucleon energy (E_f) are given by

$$E_f = \sqrt{(\mathbf{q} + \mathbf{k})^2 + M^2}. \quad (3)$$

Unfortunately, the energy of the initial state off-shell nucleon E_i is not defined in the same way in different formalisms. In addition, what is meant by the nuclear interaction energy parameter is not the same in different formalisms.

4.1 Excitation energy $[E_x]$ in the Bodek-Ritchie formalism and GENIE

Energy and momentum are strictly conserved in the formalism of BODEK-RITCHIE[17]. In electron scattering from bound protons the initial state energy E_i^P of the off-shell bound proton with momentum \mathbf{k} is defined below. The momentum is balanced by an excited (excitation energy E_x^P) $(A-1)^*$ on-shell nucleus with momentum $-\mathbf{k}$.

$$\begin{aligned} E_i^P &= M_A - \sqrt{(M_{A-1^*})^2 + \mathbf{k}^2} \\ M_{A-1^*} &= M_{A-1} + E_x^P \\ E_i^P &= M_A - \sqrt{(M_{A-1} + E_x^P)^2 + \mathbf{k}^2} \end{aligned} \quad (4)$$

$$E_i^P \approx M_A - \sqrt{(M_{A-1})^2 + \mathbf{k}^2} - E_x^P \quad (5)$$

Symbol	
$E_x^{P,N}$	Spectator Nucleus Excitation Used in spectral functions implemented in GENIE[1]
$S^{P,N}$ $= M_{A-1} + M_{p,n} - M_A$	Separation Energy Nuclear Data Tables (measured) [19, 20]
$E_m^{P,N} = S^{P,N} + E_x^{P,N}$	removal (or missing) energy used in spectral functions
$\epsilon_R^{P,N} = E_m^{P,N} + T_{A-1}$ $T_{A-1} =$ $= \sqrt{\mathbf{k}^2 + M_{A-1}^2} - M_{A-1}$ $\approx \frac{\mathbf{k}^2}{2M_{A-1}}$	interaction energy is $\epsilon_R^{P,N}$ $E_i = M - \epsilon_R^{P,N}$ used in $E_\nu^{QE-\mu}$, $Q_{QE-\mu}^2$, and Q_{QE-P}^2 , also used in effective spectral functions[8]
$\epsilon_{SM}^{(P,N)} = \epsilon_R^{P,N} + T_{av}^{P,N}$ $T = \sqrt{\mathbf{k}^2 + M^2} - M$ $\langle \mathbf{k}^2 \rangle = 0.6K_F^2$	$\epsilon_{SM}^{(P,N)}$ is Smith Moniz[11] Interaction energy $E_i = M + T - \epsilon_{SM}^{(P,N)}$ used in NEUT-NUANCE[3, 4]

Table 2. Summary of the relationships between excitation energy $E_x^{P,N}$ (used in GENIE), separation energy $S^{P,N}$, removal (missing) energy $E_m^{P,N}$ (used in spectral function measurements), relativistic interaction energy $\epsilon_R^{P,N}$ (used in the reconstruction of neutrino energy from muon kinematics only) and the Smith-Moniz interaction energy $\epsilon_{SM}^{(P,N)}$ (that should be used in NEUT-NUANCE).

This off-shell energy for the initial state proton is defined the same way for both QE scattering (final state mass = M) and inelastic scattering (final state mass = W). The interaction energy parameter in the BODEK-RITCHIE formalism is the *mean* excitation energies $\langle E_x \rangle$ of the spectator A-1 nucleus. The BODEK-RITCHIE model is implemented[18] in GENIE (although some corrections are needed as discussed in appendix B). GENIE is used by several neutrino experiments including MINERνA, MINOS NOVA and DUNE.

4.2 Removal energy $\Delta^P = \langle E_m^P \rangle$ in the effective spectral function formalism

The ground state mass of the spectator (A-1) nucleus can be expressed in terms of the mass of the initial state nucleus as follows.

$$\begin{aligned} M_A &= M_{A-1} + M_{p,n} - S^{P,N} \\ M_{A-1} &= M_A - M_{p,n} + S^{P,N} \end{aligned} \quad (6)$$

where $S^{P,N}$ is the (proton, neutron) separation energy (available in nuclear data tables). The values of S_P and S_N for various nuclei[19, 20] are given in Table 1.

In the effective spectral function formalism[8] we define Δ^P as the mean removal energy for a bound proton with momentum \mathbf{k} as follows.

$$\begin{aligned} E_i^P &= M_A - \sqrt{(M_A - M + S^P + E_x^P)^2 + \mathbf{k}^2} \\ &= M_A - \sqrt{(M_A - M + \Delta^P)^2 + \mathbf{k}^2}. \end{aligned} \quad (7)$$

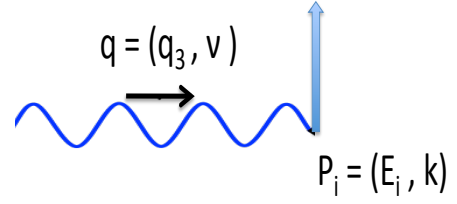


Fig. 5. Scattering from an off-shell bound nucleon of momentum k which is perpendicular to the direction of the virtual photon. This is the configuration at the *peak* of the Fermi motion smearing. At the *peak* of the distribution the z component of the nucleon momentum (k_z) is zero.

As shown in the next section, Δ^P is equal to the *mean* missing energy $\langle E_m^P \rangle$ for the 1p1h process (averaged over \mathbf{k}) measured in $ee'p$ electron scattering experiments.

4.3 Removal or Missing energy E_m in $ee'p$ experiments

In $ee'p$ high resolution electron scattering experiments the spectral function for the removal of a bound proton is typically measured as a function of missing momentum $\mathbf{p}_m = \mathbf{k}$ and missing energy E_m^P defined as follows:

$$E_i^P = M_A - \sqrt{(M_A - M + E_m^P)^2 + \mathbf{k}^2}. \quad (8)$$

The spectral function can also be measured as a function of the excitation energy $E_x^P = E_m - S^P$.

The *mean* removal energy can be identified as the *mean* missing energy $\langle E_m^P \rangle$ measured for the 1p1h process in $ee'p$ experiments.

$$\langle E_m^P \rangle = S^P + \langle E_x^P \rangle. \quad (9)$$

4.4 Interaction energy $\epsilon_R^{P,N}$

The fully relativistic expression for the interaction energy ϵ_R^P of a proton is defined as:

$$E_i^P = M - \epsilon_R^P. \quad (10)$$

For

$$E_i^P = M_A - \sqrt{(M_A - M + E_m^P)^2 + \mathbf{k}^2}, \quad (11)$$

we obtain

$$\begin{aligned} \epsilon_R^P &= E_m^P + T_{A-1} \\ &= S^P + E_x + T_{A-1}. \end{aligned} \quad (12)$$

Here, $T_{A-1} = \sqrt{\mathbf{k}^2 + M_{A-1}^2} - M_{A-1}$ is the kinetic energy of the recoiling (A-1) spectator nucleus.

For *neutrino experiments* it is the *mean* interaction energy $\langle \epsilon_R^{P,N} \rangle$ that should be used in the calculation of $E_\nu^{QE-\mu}$, $Q_{QE-\mu}^2$ (or Q_{QE-P}^2) when these quantities are reconstructed only from the muon (or proton) kinematics as discussed in Appendix D.2.

4.5 The Interaction energy in the RFG model of Moniz

In the Moniz non-relativistic analysis the initial state interacting proton is assumed to be on-shell. The on-shell energy E_i is defined as:

$$E_i = M_p + \frac{\mathbf{k}^2}{2M_p} - \epsilon_M^P.$$

Here, ϵ_M^P is the non-relativistic Moniz interaction energy. For QE scattering in a bound proton the final state proton is on-shell and has energy E_f .

$$\begin{aligned} E_f &= M_p + \frac{(\mathbf{k} + \mathbf{q})^2}{2M_p} \\ &= M_p + \frac{\mathbf{k}^2}{2M_p} + \frac{\mathbf{q}^2}{2M_p} + \frac{\mathbf{k} \cdot \mathbf{q}}{M_p}. \end{aligned}$$

Moniz uses the following non-relativistic energy conserving δ function:

$$\delta \left[\nu + \left(\frac{\mathbf{k}^2}{2M_p} - \epsilon_M^P \right) - \frac{(\mathbf{k} + \mathbf{q})^2}{2M_p} \right],$$

or

$$\delta \left[\nu - \epsilon_M^P - \frac{\mathbf{k} \cdot \mathbf{q}}{M_p} - \frac{\mathbf{q}^2}{2M_p} \right]. \quad (13)$$

As shown in Figure 5, at the location of the *peak* of the QE distribution, \mathbf{k} is perpendicular to \mathbf{q} . The published Moniz non-relativistic interaction energies ϵ_M^P are extracted from the value of ν at the *peak* of the quasielastic distribution (ν_{peak}) using the following expression.

$$\epsilon_M^P = [\epsilon_M^P] = \nu_{peak} - \frac{\mathbf{q}^2}{2M_p} = \nu_{peak} - \frac{Q^2 + \nu^2}{2M_p}. \quad (14)$$

Moniz et al. did an analysis of e-A QE scattering of 0.5 GeV electrons at a scattering angle of 60° . At these energies the quasielastic cross section is dominated by scattering on bound protons (the contribution of scattering from neutrons is small). As stated earlier, Coulomb field corrections were not taken into account in the Moniz analysis. We address these corrections in section 4.9.

In addition, equation 13 used in the Moniz analysis is non-relativistic, and energy is not conserved if ϵ_M^P is taken to be a constant which is independent of \mathbf{k} . We address relativistic corrections in section 4.11.

4.6 The Smith-Moniz formalism

Smith and Moniz[11] use on-shell relativistic kinematics as follows,

$$E_i = (\mathbf{k}^2 + M_{p,n}^2)^{1/2} - \epsilon_{SM}^{P,N}.$$

Here, we define $\epsilon_{SM}^{P,N}$ as the SMITH-MONIZ interaction energy. For QE scattering of electron on a bound proton, the final state on-shell proton energy is E_f .

$$E_f = ((\mathbf{k} + \mathbf{q})^2 + M_p^2)^{1/2}$$

For the removal of a bound proton, the SMITH-MONIZ energy conservation δ function is:

$$\delta[\nu + ((\mathbf{k}^2 + M_p^2)^{1/2} - \epsilon_{SM}^{P,N}) - ((\mathbf{k} + \mathbf{q})^2 + M_p^2)^{1/2}]. \quad (15)$$

Equation 15 is relativistic, and satisfies energy conservation only if $\epsilon_{SM}^{P,N}(k)$ is momentum dependent as follows:

$$\begin{aligned} E_i^{P,N} &= \sqrt{M_{p,n}^2 + k^2} - \epsilon_{SM}^{P,N}(k) \\ \epsilon_{SM}^{P,N}(k) &= \epsilon_R^{P,N} + T^{P,N} \\ T^{P,N} &= (\mathbf{k}^2 + M_{p,n}^2)^{1/2} - M_{p,n}. \end{aligned}$$

where $T^{P,N}$ is the interacting nucleon on-shell kinetic energy.

Smith and Moniz make the approximation that $\epsilon_{SM}^{P,N}$ is a constant (independent of \mathbf{k}), and conserve energy on average as follows:

$$\begin{aligned} \epsilon_{SM}^{P,N} &= \epsilon_R^{P,N} + T_{av} \\ T_{av} &= \langle (\mathbf{k}^2 + M_p^2)^{1/2} - M_p \rangle \\ &\approx \frac{\langle \mathbf{k}^2 \rangle}{2M_p}. \end{aligned} \quad (16)$$

For the Fermi gas model $\langle \mathbf{k}^2 \rangle = \frac{3K_F^2}{5}$.

The SMITH-MONIZ formalism with the approximation that $\epsilon_{SM}^{P,N} = \text{constant}$ is implemented in NEUT and NUANCE (which are used by the K2K/T2K and MiniBoone collaborations, respectively). Typically $\epsilon_{SM}^{P,N}$ has taken to be the value extracted in the Moniz non-relativistic analysis. As discussed below this is incorrect for several reasons.

A summary of the relationship between excitation energy $E_x^{P,N}$ (used in GENIE), measured separation energy $S_x^{P,N}$ (from nuclear data tables), removal (missing) energy $E_m^{P,N}$ (extracted from spectral functions measured ee'p experiments), relativistic interaction energy $\epsilon_R^{P,N}$ (used in the reconstruction of neutrino energy from muon kinematics only, as discussed in Appendix D.2) and the Smith-Moniz interaction energy $\epsilon_{SM}^{P,N}$ (that should be used in NEUT and NUANCE) is given in Table 2,

4.7 2p2h process

For the simple Fermi gas model only the 1p1h process is present and the interaction energy $\epsilon_R^{P,N}$ is defined in section 4.4.

For the 2p2h process that originates from short range correlations (SRC) there is a different interaction energy. Here, two correlated nucleons (typically N and P) form a quasi-deuteron about 20% of the time[16]. The off-shell initial state interacting nucleon has momentum \mathbf{k} which is balanced by an on-shell spectator nucleon with momentum $-\mathbf{k}$. In addition there is an A-2 (Z-1,N-1)* excited spectator nucleus. For the 2p2h process originating from short range correlations ϵ_{SRC}^P for a bound proton is given

by:

$$(E_i^P)_{SRC} = M_D - \sqrt{M_n + \mathbf{k}^2} - \Delta_{SRC}^{N+P} \quad (17)$$

$$(E_i^P)_{SRC} = M_p - \epsilon_{SRC}^P \quad (18)$$

$$\epsilon_{SRC}^P = \Delta_{SRC}^{A-2} + (\sqrt{M_n + \mathbf{k}^2} - M_n) \quad (19)$$

$$\Delta_{SRC}^{A-2} = S^{N+P} + E_x^{A-2}. \quad (20)$$

Here S^{N+P} is the separation energy to remove both a proton and a neutron from nucleus with atomic weight A (given in Table 1), and E_x^{N+P} is the excitation energy of the spectator (A-2) nucleus. In our analysis, we only extract the interaction energy parameters for the 1p1h process.

4.8 Coulomb field

For targets with atomic number Z greater than one we should take into account the effect of the electric field of the nucleus on the incident and scattered electrons. These corrections are called Coulomb corrections. For atomic weight A and atomic number Z the protons create an electrostatic potential $V(r)$. In the effective momentum approximation (EMA), the effective potential for an incident electron is V_{eff}

$$V(r) = \frac{3\alpha(Z)}{2R} + \frac{r\alpha(Z)}{2R^2} \quad (21)$$

$$R = 1.1A^{1/3} + 0.775A^{-1/3} \quad (22)$$

$$V_{eff} = -0.8V(r=0) = -0.8\frac{3\alpha(Z)}{2R}. \quad (23)$$

The values for $|V| = |V_{eff}|$ calculated from equation 21 agree (within errors) with values extracted from a comparison of the *peak* positions and cross sections of positron and electron QE scattering[14]. For our estimates of $|V_{eff}|$ shown in Table 3 we use the experimental values for the nuclei that were measured in ref.[14] and use equation 21 to interpolate to other nuclei.

For electrons scattering on bound nucleons the effective incident energy is $E_{eff} = E_0 + |V_{eff}|$, and the effective scattered energy is $E'_{eff} = E' + |V_{eff}|$. This implies that the effective square of the momentum transfer is increased. For positrons scattering on bound nucleons the effective incident energy is $E_{eff} = E_0 - |V_{eff}|$, and the effective scattered energy is $E'_{eff} = E' - |V_{eff}|$. This implies that the effective square of the momentum transfer is decreased.

For completeness, though not relevant in this analysis, there is also a focusing factor $F_{foc} = \frac{E_0 + |V_{eff}|}{E_0}$ that enhances the cross section for electrons and reduces the cross section for positrons. The focussing factor cancels the $1/E_0^2$ factor in the Mott cross section. Therefore, the Coulomb correction should only be applied to the structure functions W_1 and W_2 .

4.9 Coulomb corrections to the published values of ϵ_M

As mentioned earlier Coulomb corrections were not taken into account in the Moniz analysis. In our re-analysis, we apply Coulomb corrections as follows. The incident electron is assumed to be accelerated and on average has energy E_{eff} before interacting with a bound nucleon. Similarly, the scattered electron in the nucleus has energy E'_{eff} . Consequently, instead of $Q^2 = 4E_0E'\sin^2(\theta/2)$ we should use Q'^2_{eff} where

$$Q'^2_{eff} = 4(E_0 + |V_{eff}|)(E' + |V_{eff}|)\sin^2(\theta/2). \quad (24)$$

The values of the effective potential $|V_{eff}|$ for various nuclei from ref.[14] are given in column 2 of Table 3. The Coulomb corrected interaction energy ϵ_{cc}^P is determined as follows:

$$\epsilon_{cc}^P = \nu_{peak} - \frac{Q'^2_{eff} + \nu^2}{2M}. \quad (25)$$

Therefore

$$\epsilon_{cc}^P = \epsilon_M^P - \frac{Q'^2_{eff} - Q^2}{2M}. \quad (26)$$

The Moniz non-relativistic interaction energies[10] for protons before (ϵ_M^P) and after (ϵ_{cc}^P) Coulomb corrections are given in the 6th and 8th columns of Table 3. The label P indicates that it is the interaction energy for the removal of a proton (since *electron scattering* data on nuclear targets at low energy are dominated by scattering from protons). For example for $^{208}_{82}Pb$ The Moniz non-relativistic interaction energy extracted without Coulomb corrections is $\epsilon_M^P = 44$ MeV. After Coulomb corrections $\epsilon_{cc}^P = 35.2$ MeV.

4.10 Nuclear Density corrections to K_F^P and K_F^N

The Moniz published values of K_F were extracted under the assumption that the Fermi momenta for protons and neutrons are different and are related to K_F via the relations $K_F^N = K_F(2N/A)^{1/3}$ and $K_F^P = K_F(2Z/A)^{1/3}$, respectively. What is actually measured is K_F^P , and what is published is K_F . Moniz assumes that the nuclear density (nucleons per unit volume) is constant. Therefore, in the same nuclear radius R, K_F^N for neutrons is larger if N is greater than Z. Moniz used these expressions to extract the published value of K_F from the measured value of K_F^P .

We undo this correction and re-extract the measured values of K_F^P for nuclei which have a different number of neutrons and protons. The re-extracted values of K_F^P are shown in column 3 of Table 3. The values of K_F^P extracted by Moniz in 1971 are consistent with the values of K_F^P extracted from a ψ' analysis done by Maireon and Donnelly[13] in 2002 (shown in the 4th column of Table 3).

In order to obtain the values of K_F^N from the measured values of K_F^P we use the fact that the Fermi momentum is proportional to the cube root of the nuclear

e-A expt.	$\frac{A}{Z}$ Nucl.	K_F^P, K_F^N Moniz ± 5 MeV/c	K_F^P ψ' [13] fit	E_{shift} ψ' [13] fit MeV	$[\epsilon_M^P]$ pub. Moniz MeV	$ V_{\text{eff}} $ Gueye ref.[14] MeV	$[\epsilon_{cc}^P]$ Coul. corctd MeV	$[\epsilon_R^P]$ relativ. corctd [<i>peak</i>]	$\langle \text{mean} \rangle$ minus [<i>peak</i>] est.	$\langle \epsilon_R^P \rangle$ relativ. corctd $\langle \text{mean} \rangle$
Moniz[10]	${}^6_3\text{Li}$	169,169	165	15.1	17 \pm 3	1.4	16.3	15.4 \pm 3	0.0	15.4 \pm 3
Moniz	${}^{12}_6\text{C}$	221,221	228	20.0	25 \pm 3	3.1 \pm 0.25	23.6	18.0 \pm 3	7.3 \pm 2	25.3 \pm 4
Moniz	${}^{24}_{12}\text{Mg}$	235,235	230	25.0	32 \pm 3	4.8	29.4	22.0 \pm 3	(5.0 \pm 3)	27.0 \pm 4
Frascati[22]	${}^{40}_{18}\text{Ar}$	251,263		-	-	6.6	-	17.2 \pm 5	7.8 \pm 3.4	25.0 \pm 5
Moniz	${}^{40}_{20}\text{Ca}$	251,251	241	28.0	28 \pm 3	7.4 \pm 0.6	24.6	15.4 \pm 3	7.3 \pm 3.2	22.7 \pm 5
Moniz	${}^{58.7}_{28}\text{Ni}$	257,269	245	30.0	36 \pm 3	9.8	31.9	22.1 \pm 3	6.5 \pm 3.4	28.6 \pm 5
Moniz	${}^{89}_{39}\text{Y}$	243,263	245		39 \pm 3	11.6	33.6	25.6 \pm 3	(5.4 \pm 3)	31.0 \pm 4
Shell-model	${}^{90}_{50}\text{Zr}$	243,263	-		-		-	-	5.4 \pm 3	-
Moniz	${}^{118.7}_{50}\text{Sn}$	245,270	245	28.0	42 \pm 3	13.6	35.0	27.0 \pm 3	(5.0 \pm 3)	32.0 \pm 4
jlab[14]	${}^{154}_{64}\text{Gd}$	245,272	-		-	15.9 \pm 1.2	-	-	-	-
Moniz	${}^{181}_{73}\text{Ta}$	242,271	245		42 \pm 3	17.3	33.9	26.3 \pm 3	(3.0 \pm 3)	29.3 \pm 4
Moniz	${}^{208}_{82}\text{Pb}$	245,277	248	31.0	44 \pm 3	18.9 \pm 1.5	35.2	27.2 \pm 3	2.3 \pm 3	29.5 \pm 4

Table 3. A summary of our re-extractions of the interaction energy parameters from the Moniz[10] analysis. Also shown are results for ${}^{40}_{18}\text{Ar}$ from the Frascati[22] e-A inclusive experiment. All energies are in MeV. For details see section 4.13.

density. Consequently $K_F^N = C \frac{N^{1/3}}{R_N}$, and $K_F^P = C \frac{Z^{1/3}}{R_P}$, and $K_F^N = K_F^P \frac{N^{1/3} R_P}{Z^{1/3} R_N}$. For the proton and neutron radii, we use the fits for the half density radii of nuclei (in units of femtometer) given in ref.[21].

$$R_P = 1.322Z^{1/3} + 0.007N + 0.022 \quad (27)$$

$$R_N = 0.953N^{1/3} + 0.015Z + 0.774. \quad (28)$$

We only use these fits for nuclei which do not have an equal number of protons and neutrons. For nuclei which have an equal number of neutrons and protons we assume that $K_F^N = K_F^P = K_F$.

4.11 Relativistic corrections

The Moniz analysis used non-relativistic kinematics. Here we derive the relation between the *peak* relativistic interaction energy $[\epsilon_R^P]^{Moniz}$ and the Moniz non-relativistic Coulomb corrected interaction energy $[\epsilon_{cc}^P]$. For the 1p1h quasielastic electron-proton scattering process, the final state mass $W = M_p$. At the *peak* of the quasielastic distribution the proton momentum \mathbf{k} is perpendicular to \mathbf{q} , i.e. $k_z = 0$. This yields

$$\begin{aligned} E_i &= M_p - \epsilon_R^P \\ W^2 &= M_p^2 = (P_i + q)^2 = E_i^2 - \mathbf{k}^2 + 2E_i \nu_{peak} - Q^2 \\ &= (M_p - \epsilon_R^P)^2 - \mathbf{k}_T^2 + 2(M_p - \epsilon_R^P) \nu_{peak} - Q^2 \end{aligned} \quad (29)$$

or alternatively

$$\nu_{peak} + M_p - \epsilon_R^P = \sqrt{(M_p^2 + \mathbf{k}^2)}. \quad (30)$$

The above equation yields.

$$\epsilon_R^P = \frac{M_p}{M_p + \nu_{peak}} [\epsilon_{cc}^P + \frac{\nu_{peak}^2 + (\epsilon_R^P)^2 - \langle (\mathbf{k}_T^P)^2 \rangle}{2M}], \quad (31)$$

where the very small term on the right hand side $(\epsilon_R^P)^2 \approx (\epsilon_{cc}^P)^2$. For a relativistic Fermi gas distribution (and also for a Gaussian distribution with the same RMS) $\langle (\mathbf{k}_T^P)^2 \rangle = \frac{(K_F^P)^2}{2}$ for $k_z = 0$.

In the Moniz analysis the interaction energies are extracted from the position of the *peak* of the quasielastic distribution (by fitting the ν distribution to the RFG prediction). The incident electron energy is 0.5 GeV and the scattering angle is 60 degrees. The electron energy loss ν_{peak} at the *peak* position of the QE distribution is approximately 0.13 GeV, 0.135 GeV and 0.15 GeV for ${}^{12}_6\text{C}$, ${}^{58.7}_{28}\text{Ni}$ and ${}^{208}_{82}\text{Pb}$, respectively.

We use equations 12 and 31 to extract the *peak* values of the relativistically corrected *peak* interaction energies $[\epsilon_R^P]^{Moniz}$ from the values of the Moniz Coulomb corrected values $[\epsilon_{cc}^P]$. The *peak* values are shown in the 9th column of Table 3.

4.12 Interaction energy *peak* versus *mean*

We use estimates of the difference between the *mean* and *peak* interaction energy (10th column of Table 3) to calculate the fully corrected *mean* interaction energy $\langle \epsilon_R^P \rangle^{Moniz}$ shown in column 11. These are estimated from spectral function measurement or shell model binding energies as described in the sections that follow and in appendix A. (and also given in Table 4). We use square brackets (e.g. $[\epsilon_R^P]$) for *peak* values and angle brackets (e.g. $\langle \epsilon_R^P \rangle$) for the *mean* values of the interaction energies.

4.13 Summary of the reanalysis of the Moniz results

As discussed in previous sections the various steps in the re-extractions of the interaction energy parameters from the Moniz[10] analysis are shown in the columns of Table 3. Also shown are results for ${}^{40}_{18}\text{Ar}$ from the Frascati[22]

e-A inclusive experiment. The following is a summary of all the steps.

The Fermi momenta for protons K_F^P re-extracted by using the relationship between K_F^P and K_F from the original Moniz[10] 1971 paper and the Fermi momenta for neutrons K_F^N extracted from K_F^P using the expression $K_F^N = K_F^P \frac{N^{1/3} R_P}{Z^{1/3} R_N}$, are shown in column 3. The values of K_F^P extracted by Moniz in 1971 are consistent with the values of K_F^P extracted from a ψ' analysis done by Maireon and Donnelly[13] in 2002 which are shown in column 4 (and discussed in appendix E). The E_{shift} values from Maireon and Donnelly[13] are shown in column 5.

The Moniz[10] published [*peak*] interaction energies for protons (without Coulomb corrections) [ϵ_M^P] are given in column 6. The values[14] of the effective potentials [V_{eff}] used to calculate the Coulomb corrections are given in Column 7. The *peak* interaction energies for protons after the application of Coulomb corrections [ϵ_{CC}^P] are given in column 8. The *peak* relativistic interaction energies [ϵ_R^P]^{Moniz} re-extracted from the Moniz 1971 non-relativistic ϵ_{CC}^P using relativistic energy momentum conservation are shown in column 9.

Estimates of the differences between the *mean* and *peak* position of the interaction energies (also shown in Table 4 and Figure 9) are given in column 10. The differences listed in column 10 are added to the *peak* interaction energies [ϵ_R^P] in column 9 to obtain the *mean* interaction energies [ϵ_R^P]^{Moniz} shown in column 11.

5 Spectral functions and $ee'p$ experiments

In $ee'p$ experiments the following process is investigated:

$$e + A \rightarrow e' + (A - 1)^* + p_f. \quad (32)$$

Here, an electron beam is incident on a nuclear target of mass M_A . The hadronic final state consists of a proton of four momentum $p_f \equiv (E_f, \mathbf{p}_f)$ and an undetected nuclear remnant $(A - 1)^*$. Both the final state electron and the final state proton are measured. The $(A - 1)^*$ nuclear remnant can be a $(A - 1, Z - 1)$ spectator nucleus with excitation E_x^P , or a lower A nuclear remnant with additional unbound nucleons.

Within the plane wave impulse approximation (PWIA) the initial momentum \mathbf{k} of the initial state off-shell interacting nucleon can be identified with the missing momentum \mathbf{p}_m . Here we define $p_m = |\mathbf{p}_m|$ and $k = |\mathbf{k}|$

$$\mathbf{p}_m = \mathbf{k} = \mathbf{p}_f - \mathbf{q}. \quad (33)$$

The missing energy E_m is defined by the following relativistic energy conservation expression,

$$\nu + M_A = \sqrt{(M_A - M + E_m)^2 + \mathbf{p}_m^2} + E_f, \quad (34)$$

where $E_f = \sqrt{\mathbf{p}_f^2 + M_p^2}$.

The probability distribution of finding a nucleon with initial state momentum $p_m = k$ and removal energy E_m

from the target nucleus is described by the spectral function, defined as $P_{SF}(p_m, E_m) = P_{SF}(k, E_m)$. Note that for spectral functions both $P(p_m, E_m)$ and $S(p_m, E_m)$ notation are used in some publications.

The spectral functions $P_{SF}^P(k, E_m^P)$ and $P_{SF}^N(k, E_m^N)$ for neutrons and protons are two dimensional distribution in both k and E_m . Measured or theoretically calculated spectral functions for neutrons and protons can be implemented in the Monte Carlo generators. Corrections for final state interactions of the outgoing nucleon are required in the extraction of spectral functions from $ee'p$ data. The kinematical region corresponding to low missing momentum and energy is where shell model[23] states dominate[24]. Experimentally only the spectral function for protons can be measured.

In addition to the 1p1h contribution in which the residual nucleus is left in the ground or excited bound state, the measured spectral function includes contributions from nucleon-nucleon correlations in the initial state (2p2h) where there is one or more additional spectator nucleons. Spectral function measurements cannot differentiate between a spectator (A-1) nucleus and a spectator (A-2) nucleus from SRC because the 2nd final state SRC spectator nucleon is not detected. Here, we focus on the spectral function for the 1p1h process, which dominates for E_m less than 80 MeV, and ignore the spectral function for the 2p2h process which dominates at higher values of E_m .

6 Extraction of interaction energy parameters

As mentioned earlier we extract the *mean* interaction and removal energy parameters for the 1p1h process from electron scattering data using three methods.

1. From direct measurements of $\langle E_m^P \rangle$ and $\langle T \rangle$. For some nuclei, the *mean* removal energy $\langle E_m^P \rangle$ of the spectral functions measured in $ee'p$ experiments has been extracted for tests of the Koltun sum rule[15]. As discussed in section 6.1 the contribution of two nucleon corrections is minimized by restricting the analysis to $E_m^P < 80$ MeV. This is the most reliable determination of $\langle E_m^P \rangle$. We refer to this *mean* as $\langle E_m^P \rangle^{SF}$.
2. By taking the average (weighted by shell model number of nucleons) of the nucleon "level removal energies" of all shell model levels which are extracted from spectral functions measured in $ee'p$ experiments. There are uncertainties in this method originating from fact that a fraction of the nucleons ($\approx 20\%$) in each level are in a correlated state with other nucleons (leading to 2p2h final states). The fraction of such correlated nucleons is not necessary the same for all shell-model levels. We refer to this *mean* as $\langle E_m^P \rangle^{levels}$. As discussed in section 6.7, we find that the values of $\langle E_m^P \rangle^{levels}$ are consistent with $\langle E_m^P \rangle^{SF}$ for nuclei for which both are available.
3. As a check we also extract the parameters from the location (in ν) of the *peak* position of the QE distribution in e-A *inclusive* electron scattering experiments (e.g. Moniz). Parameters extracted using this method (e.g. *peak*, [E_m^P]^{Moniz}) are corrected to account for the

Source Source	$\frac{A}{Z}$ Nucl.	K_F^P, K_F^N Moniz ± 5 updated MeV/c	K_F^P ψ' fit ref.[13] MeV/c	E_{shift} ψ' fit ref.[13] MeV	$ V_{\text{eff}} $ Gueye ref.[14] MeV	ϵ_R^P (MeV) relativistic corrected		
						$[\text{peak}], \langle \text{mean} \rangle$	Diff.	
	${}^2_1\text{H}$	88,88					4.7 \pm 1, *4.7\pm1	0.0
ee'p Tokyo[27–29]	${}^6_3\text{Li}$	169,169	165	15.1	1.4	$\epsilon_R^{\text{levels}}$	18.4 \pm 3, *18.4\pm3	0.0
ee'p Tokyo[27–29]	${}^{12}_6\text{C}$	221,221	228	20.0	3.1 \pm 0.25	$\epsilon_R^{\text{levels}}$	16.9 \pm 3, 24.0 \pm 3	7.1 \pm 3.0
ee'p NIKHEF[33]	${}^{12}_6\text{C}$					$\epsilon_R^{\text{levels}}$	18.7 \pm 1, 27.1 \pm 3	8.4 \pm 3.0
ee'p Saclay[26]	${}^{12}_6\text{C}$					$\epsilon_R^{\text{levels}}$	18.9 \pm 1, 25.8 \pm 3	6.9 \pm 3.0
						$\langle \epsilon_R \rangle^{SF}$	–, 24.8 \pm 3.0	
Shell Model binding E	${}^{12}_6\text{C}$					$\epsilon_R^{\text{levels}}$	16.0, 24.9	8.9 \pm 3.0
ee'p Jlab Hall C [25]	${}^{12}_6\text{C}$					$\langle \epsilon_R \rangle^{SF}$	–, *27.5\pm3	
ee'p Jlab Hall A [31]	${}^{16}_8\text{O}$	225,225			3.4	$\epsilon_R^{\text{levels}}$	17.7 \pm 1, *24.1\pm3	6.4 \pm 1.4
Shell Model binding E	${}^{16}_8\text{O}$					$\epsilon_R^{\text{levels}}$	16.3, 23.5	7.5 \pm 3.0
ee'p Tokyo[27–29]	${}^{27}_{13}\text{Al}$	238,241	236	18.0	5.1	$\epsilon_R^{\text{levels}}$	25.6 \pm 3, 30.6\pm3	5.0 \pm 3.0
ee'p Saclay[26]	${}^{28}_{14}\text{Si}$	239,241			5.5	$\epsilon_R^{\text{levels}}$	19.9 \pm 4.2, 28.3 \pm 2	8.1 \pm 4.2
						$\langle \epsilon_R \rangle^{SF}$	–, *24.7\pm3	
${}^{40}_{20}\text{Ca} \rightarrow {}^{40}_{18}\text{Ar}$ Shell Model	${}^{40}_{18}\text{Ar}$	251,263			6.3	$\epsilon_R^{\text{levels}}$	23.7 \pm 4.1, *30.9\pm4	7.2 \pm 3.4
ee'p Tokyo[27–29]	${}^{40}_{20}\text{Ca}$	251,251	241	28.8	7.4 \pm 0.6	$\epsilon_R^{\text{levels}}$	19.3 \pm 3.2, 26.3 \pm 3	6.9 \pm 3.2
ee'p Saclay[26]	${}^{40}_{20}\text{Ca}$					$\epsilon_R^{\text{levels}}$	18.7 \pm 4.5, 27.0 \pm 3	7.7 \pm 3.8
						$\langle \epsilon_R \rangle^{SF}$	–, *28.2\pm3	
Shell-model binding E	${}^{40}_{20}\text{Ca}$					$\epsilon_R^{\text{levels}}$	16.1, 23.6	7.5 \pm 3.8
ee'p Tokyo[27–29]	${}^{50}_{23}\text{V}$	253,266			8.1	$\epsilon_R^{\text{levels}}$	18.6 \pm 3.6 *25.6\pm3	6.9 \pm 3.2
ee'p Jlab hall C [25]	${}^{56}_{26}\text{Fe}$	254,268	241	23.0	8.9 \pm 0.7	$\langle \epsilon_R \rangle^{SF}$	–, *29.6\pm3	
ee'p Saclay[26]	${}^{58}_{28}\text{Ni}$	257,269	245	30.0	9.8	$\epsilon_R^{\text{levels}}$	19.5 \pm 3.4, 25.7 \pm 3	6.5 \pm 3.4
						$\langle \epsilon_R \rangle^{SF}$	–, *25.4\pm3	
Shell-model binding E	${}^{88}_{40}\text{Zr}$	243,263			11.9 \pm 0.9	$\epsilon_R^{\text{levels}}$	19.7, 25.1	5.4 \pm 3
ee'p Jlab Hall C [25]	${}^{197}_{79}\text{Au}$	245,276	245	25.0	18.5	$\langle \epsilon_R \rangle^{SF}$	–, *25.4\pm3	
Shell Model binding E	${}^{208}_{82}\text{Pb}$	245,277	248	31.0	18.9 \pm 1.5	$\epsilon_R^{\text{levels}}$	20.5, 22.8	2.3 \pm 3

Table 4. Comparison of the *peak* $[\epsilon_R^P]^{\text{levels}}$ and *mean* $\langle \epsilon_R^P \rangle^{\text{levels}}$ interaction energies for QE electron scattering on bound protons extracted from shell-model removal energies measured in *ee'p* spectral function experiments by Tokyo[27–29], Saclay[26], Jlab Hall A[31], Jlab Hall C [25], and NIKHEF[33]. In addition we show values of the *peak* $[\epsilon_R^P]^{\text{levels}}$ and *mean* $\langle \epsilon_R^P \rangle^{\text{levels}}$ extracted from shell-model binding energies. These are compared to the values of the *mean* $\langle \epsilon_R \rangle^{SF}$ from tests of the Koltun sum rule by Saclay[26], and Jlab Hall C [25]. The value in ***bold** is the best measurement for each nucleus.

difference in the *peaks* and means of distributions to obtain the *mean* parameters e.g. $\langle E_m^P \rangle^{\text{Moniz}}$. We obtain these corrections from shell model estimates or from spectral function measurements (as described below).

In addition, using "level removal energies" we can also extract estimates of the *peak* missing energy, which we denote as $[E_m]^{\text{levels}}$, by not including the most deeply bound shell model levels in the average.

When available, we extract the interaction energy parameters using $\langle E_m^P \rangle^{SF}$ from method 1. Otherwise we use $\langle E_m^P \rangle^{\text{levels}}$ from method 2 and method 3 is used as a check. For each of the three methods, we also use the nuclear shell model to estimate difference between the removal energies for neutrons and protons as described in Appendix A.

6.1 Direct measurements of $\langle E_m^P \rangle^{SF}$ and $\langle T \rangle^{SF}$

The best estimates of the average missing energy $\langle E_m \rangle$ and average nucleon kinetic energy $\langle T \rangle$ are directly ex-

tracted from spectral function measurements in analyses that test the Koltun sum rule [15]. The Koltun's sum rule states that

$$\frac{E_0}{A} = \frac{1}{2} [\langle T \rangle^{SF} \frac{A-2}{A-1} - \langle E_m^P \rangle^{SF}], \quad (35)$$

where E_0/A is the nuclear binding energy per particle obtained from nuclear masses and includes a (small) correction for the Coulomb energy,

$$\langle T \rangle^{SF} = \int d^3k dE_m \frac{k^2}{2M} P_{SF}(k, E_m), \quad (36)$$

and

$$\langle E_m \rangle^{SF} = \int d^3k dE_m E_m P_{SF}(k, E_m). \quad (37)$$

For precise tests of the Koltun sum rule a small contribution from three-nucleon processes should taken into account.

Nucleus S^P	$^{12}_6C$ 16.0				$^{28}_{14}Si$ 11.6			$^{58}_{28}Ni$ 8.2	
$ee'p$ $\epsilon_R^P = E_m + T_{A-1}$	shell removal energy E_m^P Saclay	shell removal energy E_m^P NIKHEF	shell removal energy E_m^P Tokyo	width FWHM Tokyo	shell removal energy E_m^P Saclay		shell removal energy E_m^P Saclay		
1s _{1/2}	2	38.1±1.0	42.6±5	36.9±0.3	19.8±0.5	2	51.0	2	62.0
1p _{3/2,1/2}	4	17.5±0.4	17.3±0.4	15.5±0.1	6.9±0.1	6	32.0	6	45.0
1d _{5/2,3/2}						4	16.1±0.8	10	21.0
2s _{1/2}						2	13.8±0.5	2	14.7±0.2
1f _{7/2}								8	9.3±0.3
T_{A-1}		1.4	1.4	1.4			0.7		0.4
$\langle E_m^P \rangle^{levels}$	6	$\langle 24.4 \pm 2 \rangle$	$\langle 25.7 \pm 2 \rangle$	$\langle 22.6 \pm 3 \rangle$		14	$\langle 27.6 \pm 2 \rangle$	28	$\langle 25.3 \pm 2 \rangle$
$\langle \epsilon_R^P \rangle^{levels}$	6	$\langle 25.8 \pm 2 \rangle$	$\langle 27.1 \pm 2 \rangle$	$\langle 24.0 \pm 3 \rangle$		14	$\langle 28.3 \pm 2 \rangle$	28	$\langle 25.7 \pm 2 \rangle$
levels removed		1s	1s	1s		1s or 1s1p		1s or 1s1p	
$[E_m^P]_{1s}^{levels}$	4	[17.5±1]	[17.3±0.4]	[15.5±1]		12	[23.7±1]	26	[22.5±1]
$[E_m^P]_{1s1p}^{levels}$						6	[15.3±1]	20	[15.7±1]
$[E_m^P]_{est}^{levels}$	4	[17.5±1]	[17.3±0.4]	[15.5±1]		9	[19.5±4.2]	23	[19.1±3.4]
$[\epsilon_R^P]_{est}^{levels}$	4	[18.9±1]	[18.7±1]	[16.9±1]		12	[19.9±4.2]	20	[19.5±3.4]
$[\epsilon_R^P]$ Moniz		[18.0±3]					[na]		[22.1±3]
difference $\langle E_m^P \rangle^{levels} - [E_m^P]_{est}^{levels}$		6.9±3	8.4±3	7.1±3	(ave) (7.3)		8.1±4.2		6.2±3.4

Table 5. Results of a DPWA analysis of the "level removal energies" for different shell-model levels done by the Saclay[26] and Tokyo[27–29] $ee'p$ experiments on $^{12}_6C$, $^{28}_{14}Si$ and $^{58}_{28}Ni$. Also shown are results of our re-analysis of the Moniz[10] data. Values of the [peak] are shown in square brackets and values for the (mean) are shown in angular brackets.

Nucleus S^P	6_3Li 4.4		$^{27}_{13}Al$ 8.3		$^{40}_{20}Ca$ 8.3			$^{51}_{23}V$ 8.1			
$ee'p$ $\epsilon_R^P = E_m + T_{A-1}$	Shell removal energy E_m^P Tokyo		Shell removal energy E_m^P Tokyo		Shell removal energy E_m^P Saclay	Shell removal energy E_m^P Tokyo	width FWHM Tokyo	Shell removal energy E_m^P Tokyo	width FWHM Tokyo		
1s _{1/2}	2	22.6±0.2	2	57±3	2	56.0	59±3	34±10	2	60±3	36±11
1p _{3/2,1/2}	1	4.5±0.2	6	34±1	6	41.0	35±1	21±3	6	40±1	25±4
1d _{5/2}			4	14.0±0.6	6	*14.9±0.8	19.0±1.1	10±3	6	19.5±0.5	19±2
2s _{1/2}			1	14.3±0.2	2	11.2±0.3	14.4±0.3	13±1	2	15.1±0.2	5±2
1d _{3/2}					4	*14.9±0.8	10.9±0.7	9±1			
1f _{7/2}						*combined			7	10.3±1.1	5±3
T_{A-1}		1.8		0.7		0.5	0.5			0.4	
$\langle E_m^P \rangle^{levels}$	3	$\langle 16.6 \pm 2 \rangle$	13	$\langle 29.9 \pm 3 \rangle$	20	$\langle 26.5 \pm 3 \rangle$	$\langle 25.7 \pm 3 \rangle$		23	$\langle 25.2 \pm 3 \rangle$	
$\langle \epsilon_R^P \rangle^{levels}$	3	$\langle 18.4 \pm 2 \rangle$	13	$\langle 30.6 \pm 3 \rangle$	20	$\langle 27.0 \pm 3 \rangle$	$\langle 26.3 \pm 3 \rangle$		23	$\langle 25.6 \pm 3 \rangle$	
levels removed		none		1s		1s or 1s1p	1s or 1s1p			1s or 1s1p	
$[E_m^P]_{1s}^{levels}$			11	24.9±2	18	[23.2±2]	[22.0±2]		21	[21.9±2]	
$[E_m^P]_{1s1p}^{levels}$					12	[14.3±2]	[15.5±2]		15	[14.6±2]	
$[E_m^P]_{est}^{levels}$	3	[16.6±2]	11	24.9±2	15	[18.7±4.5]	[18.8±3.2]		21	[18.2±3.6]	
$[\epsilon_R^P]_{est}^{levels}$	3	[18.4±2]	11	[25.6±2]	18	[19.2±4.5]	[19.3±3.2]		18	[18.6±3.6]	
$[\epsilon_R^P]$ Moniz		[15.4±3]		[na]		[15.4±3]	[15.4±3]			[na]	
difference $\langle E_m^P \rangle - [E_m^P]$ (levels)		0.0		5.0±2		7.7±4.5	6.9±3.2	(ave) (7.5)		6.9±3.6	

Table 6. Results of a DPWA analysis of the "level removal energies" for different shell-model levels done by the Saclay[26] and Tokyo[27–29] $ee'p$ experiments on 6_3Li , $^{27}_{13}Al$, $^{40}_{20}Ca$ and $^{51}_{23}V$. Values of the [peak] are shown in square brackets and values for the (mean) are shown in angular brackets. Also shown are results of our re-analysis of the Moniz[10] data.

Target	Q2	$\langle T \rangle$ $E_m^P < 80$	$\langle E_m \rangle$ $E_m^P < 80$
$^{12}_6\text{C}$ Jlab Hall C [25]	0.6	15.9	26.0
	1.2	16.3	25.8
	1.8	16.0	26.6
	3.2	17.3	26.2
Jlab $\langle T \rangle^{SF}, \langle E_m \rangle^{SF}$ Saclay $\langle T \rangle^{SF}, \langle E_m \rangle^{SF}$ Saclay $\langle E_m \rangle^{levels}$ $K_F=221 \pm 5$	Ave.	16.4 ± 0.6	26.1 ± 0.4
$^{28}_{14}\text{Si}$ Saclay $\langle T \rangle^{SF}, \langle E_m \rangle^{SF}$ Saclay $\langle E_m \rangle^{levels}$ $K_F=239 \pm 5$		17.0 ± 0.6	24.0 ± 0.6
		18.1 ± 1.3	27.6 ± 2
$^{40}_{20}\text{Ca}$ Saclay $\langle T \rangle^{SF}, \langle E_m \rangle^{SF}$ Saclay $\langle E_m \rangle^{levels}$ $K_F=239 \pm 5$		16.6 ± 0.5	27.8 ± 0.5
		18.1 ± 1.3	26.5 ± 2
$^{56}_{26}\text{Fe}$ Jlab Hall C [25]	0.6	20.4	30.7
	1.2	18.1	29.4
	1.8	17.8	27.8
	3.2	19.1	28.8
Jlab $\langle T \rangle^{SF}, \langle E_m \rangle^{SF}$ $K_F=254 \pm 5$	Ave.	18.8 ± 1.0	29.2 ± 1.1
$^{58}_{28}\text{Ni}$ Saclay $\langle T \rangle^{SF}, \langle E_m \rangle^{SF}$ Saclay $\langle E_m \rangle^{levels}$ $K_F=257 \pm 5$		18.8 ± 0.7	25.0 ± 0.7
		20.9 ± 1.4	25.3 ± 2
$^{197}_{79}\text{Au}$ Jlab Hall C [25]	0.6	20.2	25.5
	1.2	18.4	25.7
	1.8	18.3	24.1
	3.2	19.4	26.1
Jlab $\langle T \rangle^{SF}, \langle E_m \rangle^{SF}$ $K_F=245 \pm 5$	Ave.	19.1 ± 0.8	25.3 ± 0.8

Table 7. Average values of the *mean* proton kinetic energy $\langle T \rangle^{SF}$ and mean missing energy $\langle E_m \rangle^{SF}$ for 1p1h final states ($E_m^P < 80$) extracted from published tests of the Koltun sum rule using spectral function (SF) measurements at Jefferson lab Hall A[25] and Saclay[26]. All energies are in MeV.

Values of $\langle E_m \rangle^{SF}$ and $\langle T \rangle^{SF}$ for the 1p1h process ($E_m^P < 80$ MeV) published by Jlab Hall C experiments[25] and by the Saclay group[26] are given in Table 7.

6.2 Spectral function measurements and "level removal energies"

Measured 2D spectral functions can be analyzed within the distorted plane wave approximation (DPWA) to extract the *peak* and *width* of the removal (missing) energy distribution E_m^P for protons for each shell model level. We

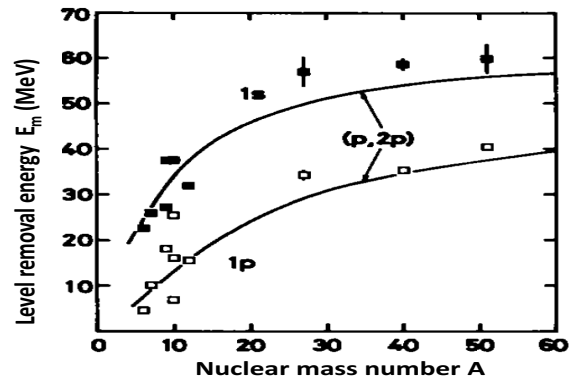


Fig. 6. Single "level removal energies" $\langle E_m^P \rangle^{1s}$ and $\langle E_m^P \rangle^{1p}$ for the **1s** and **1p** states, respectively. The data points are measurements done in $ee'p$ experiments[29]. The solid curves represent interpolations of the "level removal energies" observed in (p, 2p) experiments[30]. The "level removal energies" for the **1s** and **1p** states measured in $ee'p$ experiments are systematically higher than those observed in (p, 2p) experiments.

refer to it as the "level removal energy". In some publications it is referred to as the "shell separation energy". The energies and widths of the "level removal energies" for ^6_3Li , $^{12}_6\text{C}$, $^{17}_3\text{Al}$, $^{40}_{20}\text{Ca}$, $^{50}_{23}\text{V}$, extracted from data published by the Tokyo group[27–29] are shown in Tables 5 and 6. Also shown are the "level removal energies" for $^{12}_6\text{C}$, $^{28}_{14}\text{Si}$, $^{40}_{20}\text{Ca}$, and $^{58}_{28}\text{Ni}$, extracted from the data published by the Saclay[26] group.

We obtain an estimate of the *mean* removal energy $\langle E_m \rangle^{levels}$ for the 1p1h process by taking the average (weighted by the number of nucleons) of the "level removal energies" of all shell model levels with $E_m^P < 80$ MeV. The results of our analysis of the Saclay and Tokyo data are given in Tables 4, 5 and 6.

6.3 Peak versus mean interaction and removal energies

The "level removal energies" of the inner **1s** and **1p** levels extracted from $ee'p$ data[29] are shown Fig. 6 as a function of mass number A. The solid curves in the figure represent interpolations of the "level removal energies" observed in (p, 2p) experiments[30]. The **1s** and **1p** "level removal energies" measured in $ee'p$ experiments are systematically higher than those observed in (p, 2p) experiments. As mentioned in ref. [29] a possible explanation is that the large absorption in the (p, 2p) reaction apparently shifts the *peak* (most probably value) positions to the lower values. The **1s** and **1p** "level removal energies" seem to reach a constant value at large A. The constant values obtained in $ee'p$ experiments are about 60 MeV for the **1s** level, and about 42 MeV for the **1p** level, respectively.

As shown in Tables 5 and 6 and in Fig. 6, for the deeply bound **1s** and **1p** levels in heavy nuclei the means and widths of the removal energy distributions are large. Consequently, the *peak* in the final state electron energy distribution in inclusive QE electron scattering experiments

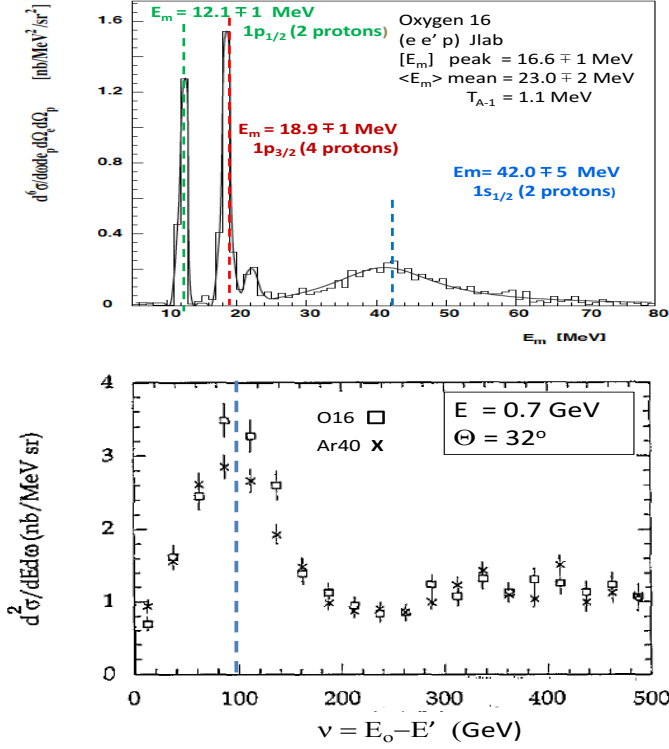


Fig. 7. Top: The spectral function for the removal of a bound proton from ^{16}O as a function of E_m^P for $\mathbf{p}_m = \mathbf{k} = 60$ MeV/c measured in Jlab Hall A[31] with 2.4 GeV incident electrons. Bottom: The measured (Frascati [22]) energy loss spectra ($\nu = E_0 - E'$) at 32° for 0.7 GeV incident electrons on ^{16}O (in squares) and ^{40}Ar (in X's), respectively. The *peaks* of the QE distributions for ^{16}O and ^{40}Ar are the same value of ($\nu_{\text{peak}} \approx 105$ MeV).

should be less sensitive to the deeply bound **1s** and **1p** levels.

As mentioned before we obtain an estimate of the *mean* removal energy $\langle E_m^P \rangle^{\text{levels}}$ for the $1p1h$ process by taking the average (weighted by the number of nucleons) of the "level removal energies" of all shell model levels with $E_m^P < 80$ MeV. In order to compare the spectral function measurements (or shell model calculations) to the Moniz measurements of the *peak* $[E_m^P]^{\text{Moniz}}$ and *peak* $[\epsilon_R^P]^{\text{Moniz}}$ we also extract an estimate of the *peak* interaction energies $[E_m^P]^{\text{levels}}$ and *peak* interaction energies $[\epsilon_R^P]^{\text{levels}}$ from the "level removal energies" as follows:

1. For N (or Z) less than 4 (^2_1H , ^6_3Li) we assume that there is no difference between the *peak* and the *mean*.
2. For $5 < N$ (or Z) < 14 ($^{12}_6\text{C}$, $^{16}_8\text{O}$, $^{27}_{13}\text{Al}$) we use the *mean* without the **1s** state (truncated *mean*).
3. For $13 < N$ (or Z) < 30 ($^{28}_{14}\text{Si}$, $^{40}_{18}\text{Ar}$, $^{40}_{20}\text{Ca}$, $^{50}_{23}\text{V}$, $^{59}_{28}\text{Ni}$) we take the average of the truncated *mean* without the **1s** state and the truncated *mean* without both the **1s** and **1p** states. We take half of the difference between these two truncated means as the systematic error in the estimate of the *peak* removal energy.

4. For N (or Z) > 30 ($^{88}_{40}\text{Zr}$, $^{197}_{79}\text{Au}$, $^{208}_{82}\text{Pb}$) we take the truncated *mean* without both **1s** and **1p** states.

Using the algorithm above we extract the *peak* of the removal (missing) energies $[E_m^P]^{\text{levels}}$ and *peak* interaction energies $[\epsilon_R^P]^{\text{levels}}$ for ^6_3Li , $^{12}_6\text{C}$, $^{17}_3\text{Al}$, $^{40}_{20}\text{Ca}$, $^{50}_{23}\text{V}$, from the Tokyo[27–29] data, and also for $^{12}_6\text{C}$, $^{28}_{14}\text{Si}$, $^{40}_{20}\text{Ca}$, and $^{58.7}_{28}\text{Ni}$ from the Saclay[26] data. These are shown in Tables 5 and 6.

6.4 Spectral function measurement of $^{16}_8\text{O}$

The spectral function for the removal of a bound proton from $^{16}_8\text{O}$ as a function of E_m^P for $\mathbf{p}_m = \mathbf{k} = 60$ MeV/c measured in Jlab Hall A[31] with 2.4 GeV incident electrons is shown in the top panel of Fig. 7. From this figure we extract a *mean* $\langle E_m^P \rangle^{\text{levels}} = 23.0 \pm 2$ MeV and a *peak* (average of the nucleons in the $1p$ level only) $[E_m^P]^{\text{levels}} = 16.6 \pm 1$ MeV. Using $T_{A-1} = 1.1$ MeV for $^{16}_8\text{O}$ we also obtain a *mean* $\langle \epsilon_R^P \rangle^{\text{levels}} = 24.1 \pm 2$ MeV and a *peak* $[\epsilon_R^P]^{\text{levels}} = 17.7 \pm 1$ MeV for $^{16}_8\text{O}$.

6.5 Inclusive electron scattering from $^{40}_{18}\text{Ar}$

The Frascati [22] measurements of the $\nu = E_0 - E'$ spectra for the QE scattering of electrons on $^{16}_8\text{O}$ (square markers) and on $^{40}_{18}\text{Ar}$ (X markers) are shown in the bottom panel of Fig. 7. The measurements were done with 0.7 GeV electrons at a scattering angle of 32° . The [*peaks*] of the QE distributions for $^{16}_8\text{O}$ and $^{40}_{18}\text{Ar}$ are at the same value of $\nu_{\text{peak}} \approx 105 \pm 5$ MeV. These spectra are not corrected for nuclear Coulomb effects. With Coulomb corrections the *peak* interaction energy for $^{40}_{18}\text{Ar}$ is expected to be 0.7 MeV lower than the *peak* interaction energy for $^{16}_8\text{O}$. Therefore, this measurement yields a *peak* $[\epsilon_R^P] = 17.0 \pm 5$ MeV for $^{40}_{18}\text{Ar}$.

6.6 Combining high resolution spectral function for $^{12}_6\text{C}$ from NIKHEF and Jlab data

The measured[32,33] NIKHEF high resolution spectral function for the removal of a bound proton in the $1p$ level of $^{12}_6\text{C}$ as a function of the spectator nucleus excitation energy E_x^P for $\mathbf{p}_m = \mathbf{k} = 172$ MeV/c is shown in the top panel of Fig. 8. For these data $[E_x^P] = 1.3$ MeV and $[E_m^P] = S^P + [E_x^P] = 17.3 \pm 0.4$ MeV (with $S^P = 16.0$ MeV for $^{12}_6\text{C}$). This value is consistent with $[E_m^P]^{\text{Moniz}} = 16.8 \pm 3$ MeV extracted from the Moniz data for $^{12}_6\text{C}$.

The Jlab measurement[25] of the one-dimensional spectral function for the removal of a bound proton from $^{12}_6\text{C}$ as a function of E_m^P for $Q^2 = 0.64$ GeV^2 is shown in the bottom panel of Fig. 8. The second *peak* at an average value of $E_m^P \approx 42.6 \pm 5$ MeV is for the removal of electrons from the **1s** level.

Combining the two results (weighted by the number of nucleons in each level) we obtain $\langle E_m^P \rangle^{\text{levels}} = 25.7 \pm 2$ MeV for $^{12}_6\text{C}$. Additional details are given in Table 5.

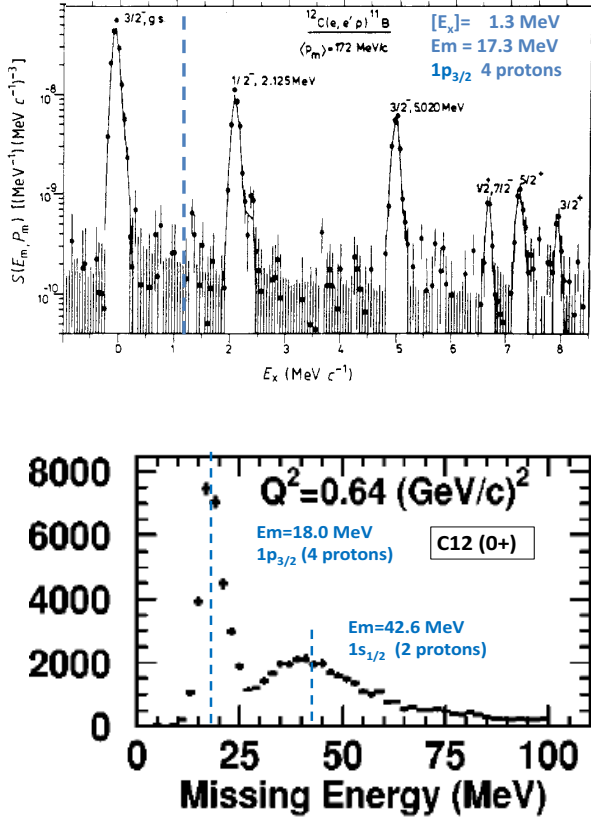


Fig. 8. Top panel: The measured[32] NIKHEF high resolution spectral function for the removal of a bound proton in the $1p$ level of ^{12}C as a function of the spectator nucleus excitation energy E_x for $p_m = k = 172$ MeV/c. Bottom panel: The Jlab measurement[25] of the one-dimensional spectral function for the removal of a bound proton from ^{12}C as a function of E_m^P for $Q^2 = 0.64$ GeV 2 .

6.7 Comparison of the three methods

Tests of the Koltun sum rule as a function of Q^2 were done by $ee'p$ experiments at Jlab Hall C[25] for ^{12}C , ^{56}Fe , and ^{197}Au . Tests of the sum rule were also reported by the Saclay[26] group for ^{12}C , ^{28}Si , ^{40}Ca , and ^{59}Ni . For both groups values of $\langle E_m^P \rangle^{SF}$ and $\langle T \rangle^{SF}$ were extracted from the measured spectral functions. The results from both groups are summarized in Table 7. We take the RMS variation with Q^2 of the Jefferson Lab Hall C data shown in Table 7 (≈ 0.5 MeV) as the statistical uncertainty in the Jlab Hall C measurements of $\langle E_m^P \rangle^{SF}$.

We use the 2.7 MeV difference in the measured values of $\langle E_m^P \rangle^{SF}$ for ^{12}C at Jefferson Lab (26.1 ± 0.4) and Saclay (23.4 ± 0.5) as the systematic error in measurements of $\langle E_m^P \rangle^{SF}$. Since $\langle E_m^P \rangle^{SF}$ is the most reliable measurement of $\langle E_m^P \rangle$, we assign ± 3 MeV as the systematic uncertainty to all measurements of $\langle E_m^P \rangle$.

The *mean* values of the interaction energies $\langle \epsilon_R^P \rangle^{SF} = \langle E_m^P \rangle^{SF} + T_{A-1}$ versus atomic number from tests of the Koltun sum rule are in good agreement with the *mean*

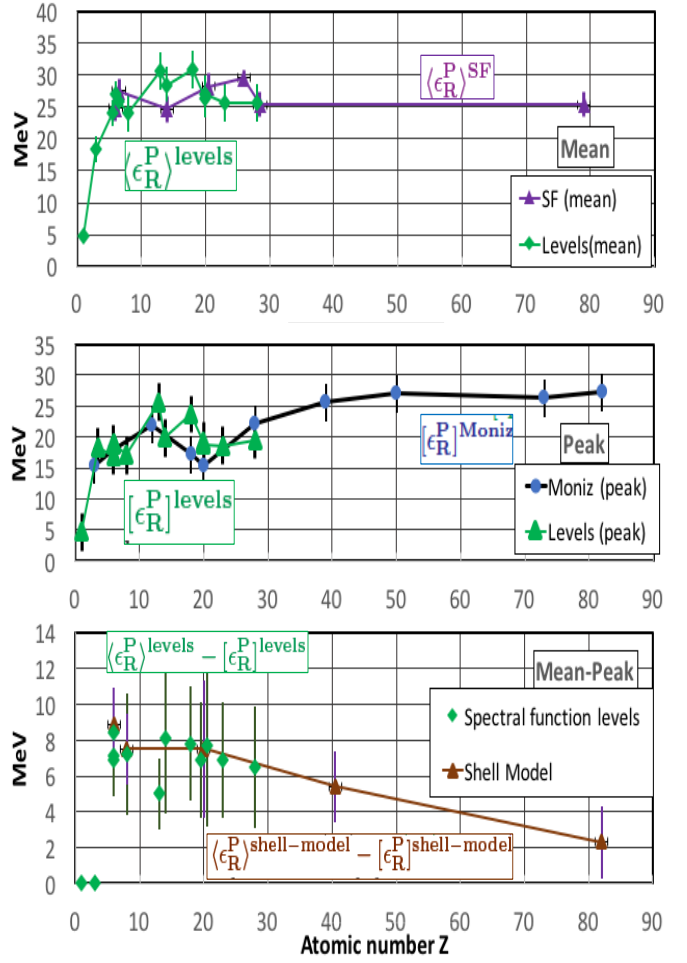


Fig. 9. Interaction energies versus atomic number Z . Top: *mean* values of $\langle \epsilon_R^P \rangle^{SF}$ from tests of the Koltun sum rule in $ee'p$ experiments (in purple) compared to *mean* values of $\langle \epsilon_R^P \rangle^{levels}$ extracted from $ee'p$ measurements of "level removal energies" (in green). Middle: *Peak* values $[\epsilon_R^P]^{levels}$ extracted from measurements of "level removal energies" in $ee'p$ experiments (in green) compared to the *peak* values of the measurements of Moniz $[\epsilon_R^P]^{Moniz}$ (in blue). Bottom: Estimates of the difference between the *mean* and *peak* interaction energies extracted from measurements of "level removal energies" (in green) compared to estimates based on the nuclear shell model (in brown). All values are taken from Table 4.

values extracted from measurements of "level removal energies" $\langle \epsilon_R^P \rangle^{levels} = \langle E_m^P \rangle^{levels} + T_{A-1}$ as shown in the top panel of Fig. 9. For example, for the Saclay data shown in Table 7 the average of the difference between $\langle E_m^P \rangle^{levels}$ and $\langle E_m^P \rangle^{SF}$ for ^{12}C , ^{28}Si , ^{40}Ca , and ^{59}Ni is 0.9 ± 1.0 MeV.

The *peak* values extracted from measurements of "level removal energies" $[\epsilon_R^P]^{levels} = [E_m^P]^{levels} + T_{A-1}$ are in good agreement with the Moniz measurements $[\epsilon_R^P]^{Moniz}$ as shown in the middle panel of Fig. 9.

Estimates of the difference between the *mean* and *peak* interaction energies extracted from "level removal energies" measured in $ee'p$ experiments $\Delta = \langle \epsilon^P \rangle^{levels} - [\epsilon^P]^{levels}$

are in good agreement with values extracted from shell model calculations as shown in the bottom panel of Fig. 9. Additional details on these shell model calculations are presented in Appendix A.

7 Extraction of interaction and excitation energies for NEUT and GENIE

We extract values of the *mean* Smith-Moniz interaction energies for protons and neutrons $\langle \epsilon_{SM}^{P,N} \rangle$ for use in the NEUT MC generator. We also extract values of the *mean* excitation energies for protons and neutrons $\langle E_x^{P,N} \rangle$ for use in the GENIE MC generator. Both are extracted from the *mean* interaction energies for protons $\langle \epsilon_R^P \rangle$ for each nucleus using the equations summarized in Table 2.

For nuclei for which we have several measurements we select the measurement that we consider to be the most reliable measurement for each nucleus. The results are presented in Table 8 and also shown in Fig 10.

7.1 Parameters that are used in the extraction

The parameters that are used in the extraction of the interaction and excitation energies for NEUT and GENIE are given in Table 9.

The average kinetic energies $T^{P,N}$ for protons and neutrons in each nucleus are given in column 2 of Table 9. Here we use the Fermi gas momentum distribution for which $\langle k^2 \rangle = 0.6 K_F^2$. The average kinetic energies $T_{A-1}^{P,N}$ for the (A-1) spectator nuclei are given in column 3.

The *mean* relativistic interaction energies for protons $\langle \epsilon_R^P \rangle$ and neutrons $\langle \epsilon_R^N \rangle$ that should be used to extract the neutrino energy and Q^2 from muon only (or proton only) measured momenta and angles (as discussed in an Appendix D) are given in column 4.

The *mean* Smith-Moniz interaction energies for protons $\langle \epsilon_{SM}^P \rangle$ and neutrons $\langle \epsilon_{SM}^N \rangle$, which compensate (on average) for the on-shell initial state energy definition in the Smith-Moniz model are given in column 5. The Smith-Moniz model is implemented in NEUT and NUANCE.

The 6th and 7th column show the separation energies for protons S^P and neutrons S^N and the difference $S^P - S^N$. The 8th column shows the *mean* excitation energies of the spectator (A-1) nucleus $\langle E_x^{P,N} \rangle$ after the removal of a bound proton or neutron. These are used in the BODEK-RITCHIE model which is implemented in GENIE.

The *mean* removal energies for neutrons and protons $\langle E_m^{P,N} \rangle = S^{P,N} + E_x^{P,N}$ are given in column 9.

The neutron parameters are derived from proton parameters by using the difference in the *mean* removal energies between neutrons and protons which are given in column 10. For the difference between neutrons and protons in carbon, oxygen, argon, calcium and lead we use the nuclear shell model. For the other nuclei we assume that $\langle E_m^N \rangle = \langle E_m^P \rangle = (S^P - S^N)$ (shown in parenthesis in column 10).

The *mean* interaction energies, excitation energies and Smith-Moniz interaction energies as a function of atomic number Z are shown in Fig. 10.

The light blue squares (dashed light blue line) and dark blue diamonds show the *mean* excitation energies $\langle E_x^P \rangle$ and $\langle E_x^N \rangle$ for protons and neutrons, respectively that should be used in GENIE.

The solid green lines and the solid red lines are the *mean* interactions energies $\langle \epsilon_R^P \rangle$ and $\langle \epsilon_R^N \rangle$ for protons and neutrons, respectively that should be used for calculating the kinematics of a QE neutrino interactions from measured momenta of the final state muon or nucleon only.

The green circles (dashed green line) and the red squares (dashed red line) are the *mean* Smith-Moniz interaction energies $\langle \epsilon_{SM}^P \rangle$ and $\langle \epsilon_{SM}^N \rangle$ for protons and neutrons, respectively that should be used in NEUT and NUANCE.

8 Conclusion

We provide updated values for the *mean* interaction energies, removal energies and excitation energies of protons and neutrons bound in nuclei. Different values of interaction energy parameters should be used for GENIE and NEUT/NUANCE. With these updated values, the *mean* reconstructed neutrino energy and other kinematic variables in neutrino MC generators are modeled with less bias.

9 Acknowledgments

Special thanks to Professors Frank Wolfs (University of Rochester), Kevin McFarland (University of Rochester), B. Alex Brown (Michigan State), Eric Christy (Hampton U.) for useful discussions. This work was supported by the US department of energy

A Input from shell model calculations

A.1 Difference between neutrons and protons for ${}^8_{12}C$ and ${}^{16}_8O$

For nuclei which have the same number of neutrons and protons we expect that the excitation energy $E_x^{P,N}$ spectrum for protons and neutrons to be approximately the same ($E_x^{P,N} \approx E_x^{N,P}$). Since $E_m^{P,N} = S^{P,N} + E_x^{P,N}$ the difference in the average removal energies for neutrons and protons is approximately equal to the difference in separation energies $S^N - S^P$. By definition, the single particle binding energy of the least bound state is equal to the separation energy, The differences in the separation energies between neutrons and protons ($S^N - S^P$) bound in ${}^8_{12}C$ and ${}^{16}_8O$ are of 2.7 MeV and 3.6 MeV, respectively.

More generally, a better estimate of the difference between the average removal energies for neutrons and protons can be obtained from the nuclear shell model. The single nucleon removal energy $(E_m^{P,N})^{shell-model-level}$ for a nucleon in a given shell-model level is close (somewhat

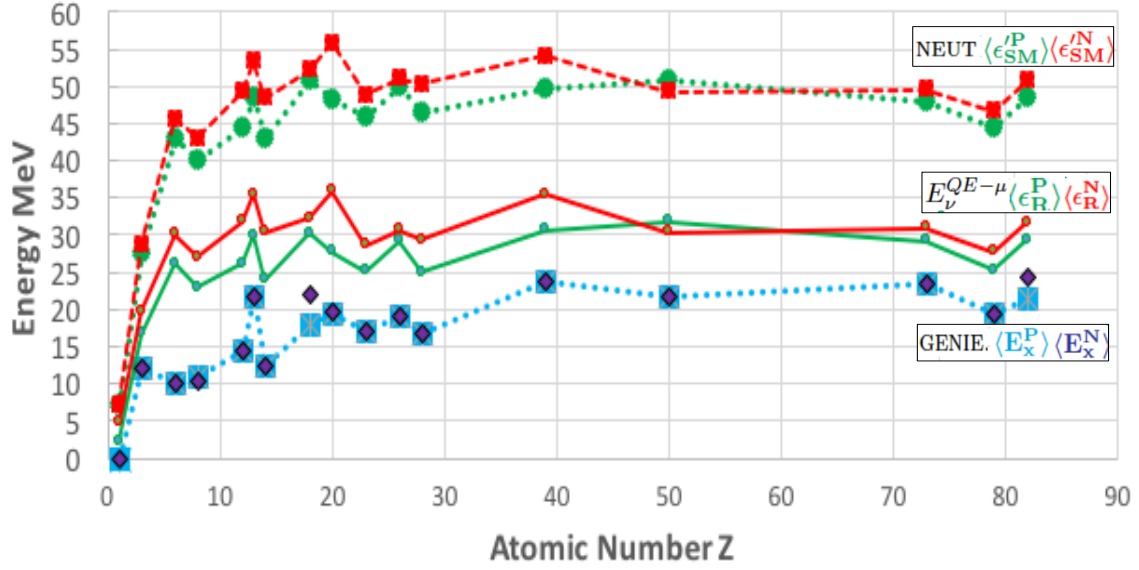


Fig. 10. interaction energy parameters versus atomic number Z . The light blue squares (dashed light blue line) and dark blue diamonds are the *mean* excitation energies $\langle E_x^P \rangle$ and $\langle E_x^N \rangle$ for protons and neutrons, respectively to be used in GENIE. The solid green lines and the solid red lines are the *mean* interactions energies $\langle \epsilon_R^P \rangle$ and $\langle \epsilon_R^N \rangle$ for protons and neutrons, respectively to be used for calculating the kinematics of a QE neutrino interactions only from the measured momentum of the final state muon or proton. The green circles (dashed green line) and the red squares (dashed red line) are the *mean* Smith-Moniz interaction energies $\langle \epsilon_{SM}^P \rangle$ and $\langle \epsilon_{SM}^N \rangle$ for protons and neutrons, respectively that should be used in NEUT and NUANCE.

${}^A_Z Nucl$	$\langle \epsilon_R^{P,N} \rangle$ relativ. corected	$\langle \epsilon_{SM}^{P,N} \rangle$ SMITH- MONIZ	$\langle E_x^{P,N} \rangle$ BODEK- RITCHIE	$\langle E_m^{P,N} \rangle$ <i>mean</i>	Measurement method used	
	$E_m + T_{A-1}^{P,N}$	$\epsilon_R^{P,N} + T$	$E_m^{P,N} - S^{P,N}$			
	use for $E_\nu^{QE-\mu}$ $Q_{QE-\mu}^2$ Q_{QE-P}^2 $\langle \epsilon_R^P \rangle$ $\langle \epsilon_R^N \rangle$	used in NEUT interaction energy $\langle \epsilon_{SM}^P \rangle, \langle \epsilon_{SM}^N \rangle$	used in GENIE excitation energy $\langle E_x^P \rangle, \langle E_x^N \rangle$	<i>mean</i> $\langle E_m^P \rangle, \langle E_m^N \rangle$		
$({}^2_1H)$	4.7	4.7	7.2, 7.2	0.0, 0.0	2.2, 2.2	Binding energy
6_3Li	18.4 ± 3	19.7 ± 3	27.5, 28.8	12.2, 12.2	16.6, 17.9	$\langle \epsilon_R \rangle^{levels}$ Tokyo[27–29]
${}^{12}_6C$	27.5 ± 3	30.1 ± 3	43.0, 45.6	10.1, 10.0	26.1, 28.7	Koltun SR $\langle \epsilon_R \rangle^{SF}$ Jlab Hall C[25]
${}^{16}_8O$	24.1 ± 3	27.0 ± 3	40.1, 43.0	10.9, 10.2	23.0, 25.9	$\langle \epsilon_R \rangle^{levels}$ Jlab Hall A[31]
${}^{24}_{12}Mg$	27.0 ± 3	31.8 ± 3	44.5, 49.3	14.5, 14.5	26.2, 31.0	updated $\langle \epsilon_R^P \rangle^{Moniz}$ [10]
${}^{27}_{13}Al$	30.6 ± 3	35.4 ± 4	48.5, 53.3	21.6, 21.6	29.9, 34.7	$\langle \epsilon_R \rangle^{levels}$ Tokyo[27–29]
${}^{28}_{14}Si$	24.7 ± 3	30.3 ± 3	42.8, 48.4	12.4, 12.4	24.0, 29.6	Koltun SR $\langle \epsilon_R \rangle^{SF}$ Saclay[26]
${}^{40}_{18}Ar$	30.9 ± 4	32.3 ± 4	50.8, 52.2	17.8, 21.8	30.2, 31.7	$\langle \epsilon_R \rangle^{levels}$ Tokyo[27–29] + Shell model
${}^{40}_{20}Ca$	28.2 ± 3	35.9 ± 4	48.1, 55.8	19.4, 19.8	27.7, 35.4	Koltun SR $\langle \epsilon_R \rangle^{SF}$ Saclay[26]
${}^{50}_{23}V$	25.6 ± 3 ,	28.6 ± 4	45.8, 48.8	17.0, 17.0	25.1, 28.1	$\langle \epsilon_R \rangle^{levels}$ Tokyo[27–29]
${}^{56}_{26}Fe$	29.6 ± 3	30.6 ± 3	50.0, 51.0	19.0, 19.0	29.2, 30.2	Koltun SR $\langle \epsilon_R \rangle^{SF}$ Jlab Hall C[25]
${}^{58.7}_{28}Ni$	25.4 ± 3	29.4 ± 3	46.3, 50.3	16.8, 16.8	25.0, 29.0	Koltun SR $\langle \epsilon_R \rangle^{SF}$ Saclay[26]
${}^{89}_{39}Y$	31.0 ± 3	35.4 ± 3	49.7, 54.1	23.6, 23.6	30.7, 35.1	updated $\langle \epsilon_R^P \rangle^{Moniz}$ [10]
${}^{118.7}_{50}Sn$	32.0 ± 3	30.4 ± 3	50.9, 49.3	21.7, 21.7	31.8, 30.2	updated $\langle \epsilon_R^P \rangle^{Moniz}$ [10]
${}^{181}_{73}Ta$	29.3 ± 3	31.0 ± 3	47.8, 49.5	23.3, 23.3	29.2, 39.9	updated $\langle \epsilon_R^P \rangle^{Moniz}$ [10]
${}^{197}_{79}Au$	25.4 ± 3	27.7 ± 3	44.4, 46.7	19.5, 19.5	25.3, 27.6	Koltun SR $\langle \epsilon_R \rangle^{SF}$ Jlab Hall C[25]
${}^{208}_{82}Pb$	29.5 ± 3	31.7 ± 3	48.5, 50.7	21.4, 24.2	29.4, 31.6	updated $\langle \epsilon_R^P \rangle^{Moniz}$ [10]

Table 8. Summary of the *mean* excitation energies, interaction energies and the Smith-Moniz interaction energies. The uncertainties are between 3 and 4 MeV. All values are in MeV. For additional details, see Table 9 and details in section 7 and Appendix A.

${}^A_Z Nucl$	$mean$ $\langle T^{P,N} \rangle$	$mean$ $T_{A-1}^{P,N}$	$\langle \epsilon_R^{P,N} \rangle$ relativ. corrected $E_m + T_{A-1}^{P,N}$	$\langle \epsilon_{SM}^{P,N} \rangle$ SMITH- MONIZ $\epsilon_R^{P,N} + T$	Separation Energies	ΔS N-P	$\langle E_x^{P,N} \rangle$ BODEK- RITCHIE $E_m^{P,N} - S^{P,N}$	$\langle E_m^{P,N} \rangle$ $mean$	ΔE_m N-P $mean$
	nucleon $\langle KE \rangle$ T^P, T^N	A-1 nucleus $\langle KE \rangle$ P, N	use for $E_\nu^{QE-\mu}$ $Q_{QE-\mu}^2$ Q_{QE-P}^2 $\langle \epsilon_R^P \rangle, \langle \epsilon_R^N \rangle$	use in NEUT interaction energy $\langle \epsilon_{SM}^P \rangle, \langle \epsilon_{SM}^N \rangle$	S^P, S^N	diff $S^N - S^P$	use in GENIE excitation energy $\langle E_x^P \rangle, \langle E_x^N \rangle$	$mean$ E_m^P, E_m^N	diff $E_m^N - E_m^P$
$({}^2_1H)$	2.5, 2.5	2.5, 2.5	4.7, 4.7	7.2, 7.2	2.2, 2.2	0.0	0.0, 0.0	2.2, 2.2	0.0
6_3Li	9.1, 9.1	1.8, 1.8	18.4, 19.7	27.5, 28.8	4.4, 5.7	1.3	12.2, 12.2	16.6, 17.9	(1.3)
${}^{12}_6C$	15.5, 15.5	1.4, 1.4	27.5, 30.1	43.0, 45.6	16.0, 18.7	2.7	10.1, 10.0	26.1, 28.7	2.6
${}^{16}_8O$	16.0, 16.0	1.1, 1.1	24.1, 27.0	40.1, 43.0	12.1, 15.7	3.6	10.9, 10.2	23.0, 25.9	2.9
${}^{24}_{12}Mg$	17.5, 17.5	0.8, 0.8	27.0, 31.8	44.5, 49.3	11.7, 16.5	4.8	14.5, 14.5	26.2, 31.0	(4.8)
${}^{27}_{13}Al$	17.9, 18.4	0.7, 0.7	30.6, 35.4	48.5, 53.3	8.3, 13.1	4.8	21.6, 21.6	29.9, 34.7	(4.8)
${}^{28}_{14}Si$	18.1, 18.4	0.7, 0.7	24.7, 30.3	42.8, 48.4	11.6, 17.2	5.6	12.4, 12.4	24.0, 29.6	(5.6)
${}^{40}_{18}Ar$	19.9, 21.9	0.5, 0.6	30.9, 32.3	50.8, 52.2	12.5, 9.9	-2.6	17.8, 22.1	30.2, 31.7	1.4
${}^{40}_{20}Ca$	19.9, 19.9	0.5, 0.5	28.2, 35.9	48.1, 55.8	8.3, 15.6	7.3	19.4, 19.8	27.7, 35.4	7.7
${}^{50}_{23}V$	20.2, 22.4	0.4, 0.5	25.6, 28.6	45.8, 48.8	8.1, 11.1	3.0	17.0, 17.0	25.1, 28.1	(3.0)
${}^{56}_{26}Fe$	20.4, 22.6	0.4, 0.4	29.6, 30.6	50.0, 51.0	10.2, 11.2	1.0	19.0, 19.0	29.2, 30.2	(1.0)
${}^{58.7}_{28}Ni$	20.9, 22.8	0.4, 0.4	25.4, 29.4	46.3, 50.3	8.2, 12.2	4.0	16.8, 16.8	25.0, 29.0	(4.0)
${}^{89}_{39}Y$	18.7, 21.9	0.2, 0.3	31.0, 35.4	49.7, 54.1	7.1, 11.5	4.4	23.6, 23.6	30.7, 35.1	(4.4)
${}^{88}_{40}Zr$					8.4, 12.0	3.6			1.9
${}^{118.7}_{50}Sn$	18.9, 23.1	0.2, 0.2	32.0, 30.4	50.9, 49.3	10.1, 8.5	-1.6	21.7, 21.7	31.8, 30.2	(-1.6)
${}^{181}_{73}Ta$	18.5, 23.2	0.1, 0.1	29.3, 31.0	47.8, 49.5	5.9, 7.6	1.7	23.3, 23.3	29.2, 39.9	(1.7)
${}^{197}_{79}Au$	19.0, 24.0	0.1, 0.1	25.4, 27.7	44.4, 46.7	5.8, 8.1	2.3	19.5, 19.5	25.3, 27.6	(2.3)
${}^{208}_{82}Pb \rightarrow$	19.0, 24.2	0.1, 0.1	29.5, 31.7	48.5, 50.7	8.0, 7.4	-0.6	21.4, 24.2	29.4, 31.6	2.2

Table 9. Additional information on the parameters that enter into the extractions of excitation $\langle E_m^{P,N} \rangle$, interaction $\langle \epsilon_R^{P,N} \rangle$, and the Smith-Moniz interaction $\langle \epsilon_{SM}^N \rangle$ energy presented in Table 8. Details in section 7 and Appendix A. All values are in MeV.

larger) to the single nucleon binding energy for that level. Consequently, the difference in the average removal energies for neutrons and protons for a nucleus $\langle E_m^P \rangle - \langle E_m^N \rangle$ is also approximately equal to the difference in the average binding energies.

The binding energies of different shell-model levels[34] for ${}^{12}_6C$ and ${}^{16}_8O$ are shown in Table A1. When available, the experimental values shown in *italics* are used. The differences between the *means* of the nucleon binding energies in all shell-model levels for neutrons and protons is 2.6 and 2.9 MeV for ${}^{12}_6C$ and ${}^{16}_8O$, respectively. As expected these values are similar (within 1 MeV) to the differences in the separation energies for neutrons and protons ($S^N - S^P$) bound in ${}^{12}_6C$ and ${}^{16}_8O$ of 2.7 and 3.6 MeV, respectively.

As shown in the last row of Table A1, the difference between the *mean* and *peak* removal energies for protons extracted from the measured "level removal energies" for ${}^{16}_8O$ of 6.4 ± 1 MeV is consistent with 7.5 ± 1 MeV estimated from the shell-model calculations.

A.2 Difference between neutrons and protons for ${}^{40}_{20}Ca$

The theoretical[34] shell model energy levels for *protons* bound in ${}^{40}_{20}Ca$ are shown in the third column of Table A2. Here, the binding energy of the least bound state has been

set to the value of the separation energy. The measured values of the binding energies are shown in *italics* and are used when available. The theoretical shell model energy levels for *neutrons* bound in ${}^{40}_{20}Ca$ [34] are shown in column 6. The *mean* "level removal energies" for shell-model states measured by the Tokyo *ee'P* experiment[29] are shown in column 4. The differences between the measured removal energies and shell-model binding energies for protons are shown in column 5.

The *ee'N* "level removal energies" for neutron levels (in column 7) are estimated by adding the difference for protons (column 5) to the shell-model level binding energies for neutrons (column 6).

As shown in last column of Table A2, the difference between the *mean* removal energies for *neutrons* and *protons* in calcium is 7.8 ± 2 GeV. This is consistent with $S^N - S^P = 7.3$ GeV as expected for a nucleus that has the same number of protons and neutrons.

As shown in the bottom row of Table A2, the difference between the *mean* and *peak* removal energies for protons extracted from the measured "level removal energies" for ${}^{40}_{20}Ca$ of 6.9 ± 3.8 MeV is consistent with 7.5 ± 3.8 MeV estimated from our shell-model calculation.

T_{A-1}	$^{12}_6\text{C}$	proton 1.4	neutron 1.4	N-P Diff	$^{16}_8\text{O}$	proton 1.1	proton 1.1	neutron 1.1	N-P Diff
		binding energy	binding energy			Jlab shell removal energy	binding energy	binding energy	
S^P, S^N		16.0	18.7	2.7		12.1	12.1	15.7	3.6
$1s_{1/2}$	2	42.6	43.9	1.3	2	42±2	45.0 (40±8)	47.0	2.0
$1p_{3/2}$	4	<i>16.0</i>	<i>18.7</i>	2.7	4	18.9±0.5	<i>18.4</i>	<i>21.8</i>	3.4
$1p_{1/2}$	2				2	12.1±0.5	<i>12.1</i>	<i>15.7</i>	3.6
mean $\langle E_m \rangle$, BE	6	$\langle 24.9 \rangle$	$\langle 27.1 \rangle$	2.6	8	$\langle 23.0 \pm 2 \rangle$	$\langle 23.5 \rangle$	$\langle 26.6 \rangle$	2.9 ± 1
levels not included <i>peak $[E_m]$, BE</i>		1s	1s			1s	1s	1s	
	4	[16.0]	[18.7]	2.7	6	[16.6]	[16.3]	[19.8]	3.5±1
mean $\langle E_m \rangle$-<i>peak $[E_m]$</i>	$^{12}_6\text{C}$				$^{16}_8\text{O}$	6.4±1	7.5±1		

Table A1. Shell-model single particle binding energies for $^{12}_8\text{C}$ and $^{16}_8\text{O}$ from ref.[34]. When available, the experimental values shown in *italics* are used. The difference between the *mean* removal energies $\langle E_m^{P,N} \rangle$ for *neutrons* and *protons* can be approximated by the difference in the weighted average of the single particle binding energies of all shell-model levels. We obtain differences of 2.6 and 2.9 MeV for $^{12}_8\text{C}$ and $^{16}_8\text{O}$, respectively. These differences are close to the corresponding differences in separation energies of neutrons and protons (S^N-S^P) of 2.7 and 3.6 MeV, for $^{12}_8\text{C}$ and $^{16}_8\text{O}$, respectively.

$^{40}_{20}\text{Ca}$	proton binding energy	proton shell removal <i>ee'p</i> Tokyo[29]	Diff. Shell energy	neutron binding energy	neutron shell removal (<i>ee'N</i>)	N-P BE	
$T_{A-1}=0.5$	BE	<i>measured</i>	less BE	BE	<i>estimated</i>	Diff	
S_p, S_n	8.3			15.6		7.3	
$1s_{1/2}$ (<i>measured</i>)	2 <i>50±11</i>	<i>59±3</i>	2.2	66.0	(<i>68.2</i>)	3.2	
$1p_{3/2}$	4 36.0			43.7		7.7	
$1p_{1/2}$ (<i>measured</i>)	2 <i>31.1</i> <i>34±6</i>	<i>35±1</i>	0.6	39.0 (42.1)	(<i>42.7</i>)	7.9 (8.1)	
$1d_{5/2}$	6 14.4	<i>19.0±1.1</i>	4.6	22.3	(<i>26.9</i>)	8.4	
$2s_{1/2}$	2 10.9	<i>14.4±0.3</i>	3.5	18.1	(<i>21.6</i>)	7.2	
$1d_{3/2}$	4 <i>8.3</i>	<i>10.9±0.7</i>	2.6	15.6	(<i>18.2</i>)	7.3	
mean $\langle E_m^P \rangle$ levels, BE	20	$\langle 23.1 \rangle$	$\langle 25.7 \rangle \pm 3$	2.6	$\langle 30.9 \rangle$	$\langle 33.5 \rangle \pm 4$	7.8±2
mean $\langle \epsilon_R^P \rangle$ levels, BE	20	$\langle 23.6 \rangle$	$\langle 26.3 \rangle \pm 3$	2.6	$\langle 31.4 \rangle$	$\langle 34.0 \rangle \pm 4$	7.8±2
levels removed <i>peak $[E_m^P]_{levels}$</i>	18	1s or 1s1p [19.4]	1s or 1s1p [22.0]±2		1s or 1s1p [26.9]	1s or 1s1p [29.6]	
<i>peak $[E_m^P]_{1s1p}$</i>	12	[11.9]	[15.5]±2		[19.4]	[23.1]	
<i>peak $[E_m^P]_{est}$</i>	15	[15.7]	[18.8]±3.5	3.1	[23.2]	[26.3]	7.5±2
<i>peak $[\epsilon_R^P]_{est}$</i>	15	[16.2]	[19.3]±3.5	3.1	[23.7]	[26.8]	7.5±2
<i>peak $[\epsilon_R^P]$ Moniz</i>			[15.4]±3.0				
difference mean $\langle E_m \rangle$-<i>peak $[E_m]$</i>		7.5±3.8	6.9±3.5				

Table A2. Shell-model levels binding energies for $^{40}_{20}\text{Ca}$ from ref.[34]. When available, the experimental values shown in *italics* are used. Also shown are the measured "level removal energy" E_m for each proton level from the Tokyo *ee'p* experiment[29]. The "level removal energies" for neutrons are estimated by combining information from the shell model energy level calculations for $^{40}_{20}\text{Ca}$ with measured (*ee'P*) "level removal energies" for protons in $^{40}_{20}\text{Ca}$. For details see section A.2. All energies are in MeV.

A.3 Proton and neutron removal energies for $^{40}_{18}\text{Ar}$

The theoretical shell-model level binding energies[34] for proton and neutrons in $^{40}_{18}\text{Ar}$ are given in columns 3 and 7 of Table A3, respectively. When available, the experimental values shown in *italics* are used. The difference between the experimental "level removal energies" and shell-model

level binding energies for protons in $^{40}_{20}\text{Ca}$ is given in column 4.

The (*ee'p*) "level removal energies" for protons in $^{40}_{18}\text{Ar}$ (column 5) are estimated by adding the difference between the experimental "level removal energies" and shell-model level binding energies for $^{40}_{20}\text{Ca}$ (column 4) to the shell-model binding energies for protons in $^{40}_{18}\text{Ar}$ (column 3).

$^{40}_{18}\text{Ar}$ $S_p=12.5, S_n=9.9$ $T_{A-1}=0.5$	$^{40}_{18}\text{Ar}$	$^{40}_{18}\text{Ar}$ proton binding energy BE	$^{40}_{20}\text{Ca}$ Diff level minus BE	$^{40}_{18}\text{Ar}$ proton level removal <i>est.</i>	$^{40}_{18}\text{Ar}$	$^{40}_{18}\text{Ar}$ neutron binding energy BE	$^{40}_{18}\text{Ar}$ neutron level removal <i>est.</i>	$^{40}_{18}\text{Ar}$ N-P BE Diff	$^{40}_{18}\text{Ar}$ N-P removal energy Diff
S^P, S^N		12.5				9.9			-2.6
1s _{1/2}	2	58.5	2.2	(60.7)	2	66.3	(68.5)	7.8	7.8
1p _{3/2}	4	38.5			4	44.3		6.8	
1p _{1/2}	2	34.5			2	39.3		4.8	
combined		(37.2)	0.6	(37.8)		(42.7)	(43.3)	(5.5)	(5.5)
1d _{5/2}	6	17.5	4.6	(22.1)	6	22.3	(26.9)	4.8	4.8
2s _{1/2}	2	14.5	3.5	(18.0)	2	17.5	(21.0)	3.0	3.0
1d _{3/2}	2	12.5	2.6	(15.1)	4	15.8	(18.4)	3.0	3.3
1f _{7/2}					2	9.9	12.5	0.0	0.0
mean $\langle E_m \rangle^{\text{levels}}, \text{BE}$	18	(27.7)		$\langle 30.4 \rangle \pm 4$	22	$\langle 29.1 \rangle$	$\langle 31.8 \rangle \pm 4$	1.4	1.4 ±2
mean $\langle \epsilon_R \rangle^{\text{levels}}, \text{BE}$	18	(28.2)		$\langle 30.9 \rangle \pm 4$	22	$\langle 29.6 \rangle$	$\langle 32.3 \rangle \pm 4$	1.4	1.4±2
levels removed		1s or 1s1p		1s or 1s1p		1s or 1s1p	1s or 1s1p		
peak $[E_m]_{1s}^{\text{levels}}$	16	[23.9]		[26.6]	20	[25.4]	[29.8]		
peak $[E_m]_{1s1p}^{\text{levels}}$	10	[15.9]		[19.9]	14	[18.0]	[21.6]		
peak $[E_m]_{\text{est}}^{\text{levels}}$	13	[19.9]±4		[23.2]±3.4	17	[21.7]±4.6	[25.7]±4.1	1.8	2.5±2
peak $[\epsilon_R]_{\text{est}}^{\text{levels}}$	13	[20.4]±4		[23.7]±3.4	17	[22.2]±4.6	[26.2]±4.1	1.8	2.5±2
difference mean $\langle E_m \rangle - \text{peak} [E_m]$		7.8±4		7.2±3.4					

Table A3. Shell model binding energies for $^{40}_{18}\text{Ar}$ from ref.[34]. When available, the experimental values shown in *italics* are used. The "level removal energies" for protons and neutrons are estimated by combining information from the shell model energy level calculations for $^{40}_{18}\text{Ar}$ and $^{40}_{20}\text{Ca}$ with measured ($ee'P$) "level removal energies" for $^{40}_{20}\text{Ca}$. For details see section A.3.

Similarly, the $ee'N$ "level removal energies" for neutrons in $^{40}_{18}\text{Ar}$ (column 8) are estimated by adding the difference between the experimental "level removal energies" and shell-model level binding energies for protons in $^{40}_{20}\text{Ca}$ (column 4) to the shell-model binding energies for neutrons in $^{40}_{18}\text{Ar}$ (column 7).

The above estimates yield $\langle E_m^P \rangle^{\text{levels}}$ for protons in $^{40}_{18}\text{Ar}$ of 29.8 ± 3 MeV, and $\langle E_m^N \rangle^{\text{levels}}$ for neutrons in $^{40}_{18}\text{Ar}$ of 33.5 ± 3 MeV.

We find that for $^{40}_{18}\text{Ar}$, which does not have an equal number of neutrons and protons, the difference in the *mean* removal energies between neutrons and protons is

$$\langle E_m^N \rangle^{\text{levels}} - \langle E_m^P \rangle^{\text{levels}} = +1.4 \pm 2 \text{ MeV}$$

compared to $S^N - S^P = -2.6$ MeV.

A.4 Shell-model estimates for high Z nuclei

A.4.1 Peak versus mean for high Z nuclei

Two calculations of shell model energy levels for $^{16}_8\text{O}$, $^{40}_{20}\text{Ca}$, $^{90}_{40}\text{Zr}$ and $^{298}_{82}\text{Pb}$ are compared to data in reference [35]. One calculation (referred to as "Interaction I") is better at estimating the binding energies of low bound states, and another calculation (referred to as "Interaction II") is better at estimating the binding energies of deeply bound states. The estimated shell-model binding energies for $^{90}_{40}\text{Zr}$ and $^{298}_{82}\text{Pb}$ given in Table A4 are extracted from combination of experimental data and the two calculations.

Using the values of the single particle shell-model energy levels in Table A4 we estimate the differences between the *mean* binding energy and *[peak]* binding energy for protons bound in $^{90}_{40}\text{Zr}$ and $^{298}_{82}\text{Pb}$ to be 5.4 ± 2 MeV and 2.3 ± 3 , respectively. The corresponding differences for $^{89}_{39}\text{Y}$, $^{119}_{50}\text{Sn}$, and $^{181}_{73}\text{Ta}$ are obtained by interpolation between the values for $^{90}_{40}\text{Zr}$ and $^{298}_{82}\text{Pb}$. We use these estimates (given in column 10 of Table 4) to correct the *[peak]* interaction energies of the Moniz data for high Z nuclei.

A.4.2 Neutron versus proton

We also estimate the differences between the *mean* binding energies for *neutrons* and *protons* in $^{90}_{40}\text{Zr}$ and $^{298}_{82}\text{Pb}$ to be 1.9 ± 2 and 2.1 ± 2 MeV respectively. We use 2.1 ± 2 in Table 8 to estimate the *mean* interaction energy for neutrons from the values of the *mean* interaction energy for protons in $^{298}_{82}\text{Pb}$.

B Corrections to GENIE

The following should be kept in mind when using the current RFG (BODEK-RITCHIE) implementation in GENIE for neutrino experiments.

1. Note that the contribution of the separation energy to the removal energy for a bound nucleon is already accounted for in GENIE because the exact masses of the initial state nucleus of atomic number A and of

level	$^{208}_{82}Pb$ protons $S_p=8.0$ $T_{A-1}=0.1$	proton binding energy	$^{208}_{82}Pb$ neutrons $S_n=7.4$ $T_{A-1}=0.1$	neutron binding energy	$^{90}_{40}Zr$ protons $S_p=8.4$ $T_{A-1}=0.2$	proton binding energy	$^{90}_{40}Zr$ neutrons $S_n=12.0$ $T_{A-1}=0.3$	neutron binding energy
1s _{1/2}	2 →	53.4 60.0	2 →	62.9 70.0	2 →	53.2 60.0	2 →	62.1 70.0
1p _{3/2}	4	46.9	4	56.2	4	42.7	4	50.4
1p _{1/2}	2	46.4	2	55.7	2	41.3	2	49.2
1d _{5/2}	6	38.9	6	48.1	6	30.7	6	37.5
1d _{3/2}	4	37.8	4	47.0	4	27.7	4	34.7
2s _{1/2}	2	34.0	2	43.9	2	24.2	2	32.0
1f _{7/2}	8	30.6	8	39.0	8	18.1	8	24.3
1f _{5/2}	6	27.9	6	36.9	2	13.1	6	<i>13.5</i>
2p _{3/2}	4	23.1	4	32.8	6	10.0	4	<i>13.1</i>
2p _{1/2}	2	22.2	2	31.9	4	<i>8.4</i>	2	<i>12.6</i>
1g _{9/2}	10	<i>15.4</i>	10	29.2			10	<i>12.0</i>
1g _{7/2}	8	<i>11.4</i>	8	25.5				
2d _{5/2}	6	<i>9.7</i>	6	21.8				
1h _{11/2}	12	<i>9.4</i>	12	19.1				
2d _{3/2}	4	<i>8.4</i>	4	20.0				
3s _{1/2}	2	<i>8.0</i>	2	15.6				
1h _{9/2}			10	<i>9.7</i>				
2f _{7/2}			8	<i>9.0</i>				
1i _{13/2}			14	<i>8.8</i>				
3p _{3/2}			4	<i>8.3</i>				
2f _{5/2}			6	<i>8.0</i>				
3p _{1/2}			2	<i>7.4</i>				
mean (BE)	82	<22.8>	126	<24.9>	40	<24.9>	50	<26.8>
levels not included		1s1p		1s1p		1s1p		1s1p
peak [BE]	74	[20.5]	116	[22.6]	32	[19.5]	42	[21.4]
Moniz-[E _M]		27.1±3						
difference								
mean-peak		2.3±3		2.3		5.4±3		5.4
<BE^P>-<BE^N>				2.1 ± 3				1.9±3

Table A4. Theoretical[35] binding energies for $^{90}_{40}Zr$ (columns on right) and $^{208}_{82}Pb$ (columns on left). When available, the experimental values shown in *italics* are used. For details see section A.3. All energies are in MeV.

the spectator nucleus of atomic number (A-1) in the ground state are used (as discussed in section 4.1).

- For the excitation energy parameter in GENIE the *mean* values $\langle E_x^{P,N} \rangle$ from Table 9 should be used: e.g. (10.1, 10.0) MeV for $^{12}_8C$ and (10.9, 10.2) MeV for $^{16}_8O$, respectively. In several recent publications GENIE was used with an incorrect value of 34 MeV for these excitation energy parameters.
- The change in energy from the deceleration (μ^-) or acceleration (μ^+) of final state leptons in the Coulomb field of the nucleus is not taken into account. This energy (shown as $|V_{eff}|$ in Table 3) should be subtracted for μ^- (or added for μ^+) to simulate the muon energy which is measured in the detector. For example, $|V_{eff}|=3.1$ and 3.4 MeV for $^{12}_8C$ and $^{16}_8O$, respectively.
- In GENIE the excitation energy parameter $\langle E_x^{P,N} \rangle$ in GENIE is currently subtracted from the energy of the final state nucleon for QE events (or quarks for inelastic events). However, this energy is not currently subtracted from the energy of the final state lepton. Therefore, in order to conserve energy $\langle E_x^{P,N} \rangle$ should also be subtracted from the final state lepton, and all appropriate kinematic quantities such as Q^2 should be recalculated.
- The fraction of events from nucleon short-rang correlations (SRC) implemented in GENIE should be increased from the current $\approx 10\%$ to 20% which is indicated by recent *electron scattering* experiments. Note that here, the final state includes two nucleons and a different momentum distribution and final state kinematics should be used for modeling this process. In the Bodek-Ritchie RFG model which has about 10% events from SRC, this can simply be done by weighting each event with an initial nucleon momentum with $k > K_F$ by a factor of 2.5.
- In GENIE the *mean* excitation energy $\langle E_x^{P,N} \rangle$ averaged over all nucleons should be used. Alternatively, an implementation of few different momentum distributions and different excitation energies for the inner and outer shell nucleons (and also for SRC) could also be implemented.

C Corrections to NEUT

The following should be kept in mind when using the current RFG (SMITH-MONIZ) implementations in NEUT (and NUANCE) :

1. In the present implementation the *mean* values (see equation 16) for $\langle \epsilon_{SM}^{P,B} \rangle$ given in Table 9 should be used. Alternatively a better implementation would be to use \mathbf{k} dependent "interaction energy" (e.g. equation 16).
2. The change in energy from the deceleration (μ^-) or acceleration (μ^+) of final state leptons in the Coulomb field of the nucleus is not taken into account. This energy (shown as $|V_{eff}|$ in Table 3) should be subtracted for μ^- (or added for μ^+) to simulate the muon energy which is measured in the detector.
3. Accounting for the Coulomb correction to the muon energy by increasing the nuclear interaction energy parameter (as has been done in some analyses) is incorrect because it results in incorrect simulation of kinematic quantities such as Q^2 .
4. High momentum component from short-rang correlation of order 20% should be included as indicated by recent *electron scattering* experiments (and implemented in GENIE). Note that here, the final state includes two nucleons and a different momentum distribution and final state kinematics should be used for modeling this process.
5. In the SMITH-MONIZ model, the *mean* Smith-Moniz interaction energy $\langle \epsilon'_{SM} \rangle$ averaged over all nucleons should be used. Alternatively, an implementation of few different momentum distributions and different interaction energies for the inner and outer shell nucleons (and also for SRC) could be implemented.

D Reconstruction of $E_\nu^{QE-\mu}$, $Q_{QE-\mu}^2$ and Q_{QE-P}^2

In this section we update the expressions for the *mean* reconstructed neutrino energy $E_\nu^{QE-\mu}$ and square of the four-momentum transfer $Q_{QE-\mu}^2$ extracted only from the kinematics of final state muons in QE events. In addition we can also reconstruct the four momentum transfer $Q_{Q-(P,N)}^2$ from the kinematics of the final state recoil proton or neutron in QE events.

The expressions are updated to include:

1. The interaction energy parameters that should be used are the *mean* $\langle \epsilon_R^N \rangle$ and $\langle \epsilon_R^P \rangle$, for neutrons and protons, respectively.
2. The contribution of Coulomb corrections.
3. The contribution of the proton and neutron transverse momentum \mathbf{k}_T at the location of the QE *peak*.

In the derivation of the expressions we use relativistic kinematics. As discussed in section 4.4 the energies of the initial state proton or neutron are:

$$\begin{aligned} E_i^P &= M_p - \langle \epsilon_R^P \rangle, \\ E_i^N &= M_N - \langle \epsilon_R^N \rangle. \end{aligned} \quad (38)$$

We define M_n , M_p , m_μ as the neutron, proton, and muon masses. At the peak location of the QE distribution the bound neutron momentum is perpendicular to \mathbf{q} (i.e. $k_z=0$). In this case, the average of the square of transverse momenta of the neutron (proton) for a Fermi gas momentum distribution (and also for a Gaussian distribution) is $\langle \mathbf{k}_{T-N}^2 \rangle = \frac{(k_F^N)^2}{2}$ for a bound neutron in the initial state and $\langle \mathbf{k}_{T-P}^2 \rangle = \frac{(k_F^P)^2}{2}$ for bound proton in the initial state.

D.1 Using only the kinematics of the μ^-

For neutrino QE scattering we define $E'_{\mu^-} = T_{\mu^-} + m_\mu + |V_{eff}|$ as the total Coulomb corrected muon energy. The adjusted bound neutron energy in the laboratory system is $M'_n = M_n - \langle \epsilon_R^N \rangle$. We define $(M'_p)^2 = M_p^2 + \langle \mathbf{k}_{T-N}^2 \rangle$ to account for the fact that the final state proton has the same average transverse momentum as that of the initial state neutron $\langle \mathbf{k}_{T-N}^2 \rangle$ with respect to the neutrino-muon scattering plane. From energy-momentum conservation we get:

$$\begin{aligned} E_\nu &= p'_{\mu^-} \cos \theta_{\mu^-} + P_p \cos \theta_p \\ p'_{\mu^-} \sin \theta_{\mu^-} &= P_p \sin \theta_p \\ E_\nu + M'_n &= \sqrt{(P_p)^2 + (M'_p)^2}, \end{aligned} \quad (39)$$

where $p'_{\mu^-} = \sqrt{(E'_{\mu^-})^2 - m_\mu^2}$, P_p is the momentum of the final state proton in the neutrino-muon plane, and θ_p is the angle of the proton in the neutrino-muon plane. From equations 39 we obtain the following expressions.

$$\begin{aligned} E_\nu^{QE-\mu} &= \frac{2(M'_n)E'_{\mu^-} - ((M'_n)^2 + m_\mu^2 - (M'_p)^2)}{2 \cdot [(M'_n) - E'_{\mu^-} + (\sqrt{(E'_{\mu^-})^2 - m_\mu^2}) \cos \theta_{\mu^-}]} \\ Q_{QE-\mu}^2 &= -m_\mu^2 + 2E_\nu^{QE} (E'_{\mu^-} - \sqrt{(E'_{\mu^-})^2 - m_\mu^2} \cos \theta_{\mu^-}). \end{aligned} \quad (40)$$

D.1.1 Using only the kinematics of the final state proton

For QE neutrino scattering the average reconstructed square of the four-momentum transfer Q_{QE-P}^2 for QE events can be extracted from final state proton variables by using following modified expression:

$$Q_{QE-P}^2 = (M'_n)^2 - (M'_p)^2 + 2M'_n[M_p + T_p - M'_n]. \quad (41)$$

For antineutrino scattering we use the above expressions with E'_{μ^-} replaced by E'_{μ^+} , $|V_{eff}|$ replaced with $-|V_{eff}|$, M'_n is replaced with $M'_p = M_p - \langle \epsilon_R^P \rangle$, and $(M'_p)^2$ replaced with $(M'_n)^2 = M_n^2 + \langle \mathbf{k}_{T-P}^2 \rangle$ as shown below.

D.2 Using only the kinematics of the μ^+

For antineutrino QE scattering we define $E'_{\mu^+} = T_{\mu^+} + m_\mu - |V_{eff}|$ as the total Coulomb corrected muon energy.

The adjusted bound neutron energy in the laboratory system is $M'_p = M_p - \langle \epsilon_R^P \rangle$. We define $(M'_n)^2 = M_n^2 + \langle \mathbf{k}_{T-N}^2 \rangle$ to account for the fact that the final state neutron has the same average transverse momentum as that of the initial state proton $\langle \mathbf{k}_{T-P}^2 \rangle$ with respect to the antineutrino-muon scattering plane.

From energy-momentum conservation we get:

$$\begin{aligned} E_{\bar{\nu}} &= p'_{\mu+} \cos \theta_{\mu+} + P_n \cos \theta_n \\ p'_{\mu+} \sin \theta_{\mu} &= P_n \sin \theta_n \\ E_{\bar{\nu}} + M'_p &= \sqrt{(P_n)^2 + (M'_n)^2}, \end{aligned} \quad (42)$$

where $p'_{\mu+} = \sqrt{(E'_{\mu+})^2 - m_{\mu}^2}$, P_n is the momentum of the final state neutron in the antineutrino-muon plane, and θ_n is the angle of the neutron in the neutrino-muon plane. From equations 42 we obtain the following expressions.

$$E_{\bar{\nu}}^{QE-\mu+} = \frac{2(M'_p)E'_{\mu+} - ((M'_p)^2 + m_{\mu}^2 - (M'_n)^2)}{2 \cdot [(M'_p) - E'_{\mu+} + (\sqrt{(E'_{\mu+})^2 - m_{\mu}^2}) \cos \theta_{\mu+}]} \quad (43)$$

$$Q_{QE-\mu+}^2 = -m_{\mu}^2 + 2E_{\bar{\nu}}^{QE} (E'_{\mu+} - \sqrt{(E'_{\mu+})^2 - m_{\mu}^2} \cos \theta_{\mu+}).$$

D.2.1 Using only the kinematics of the final state neutron

For QE antineutrino scattering the average reconstructed square of the four-momentum transfer Q_{QE-N}^2 for QE events can be extracted from final state neutron variables by using following modified expression.

$$Q_{QE-N}^2 = (M'_p)^2 - (M'_n)^2 + 2M'_p[M_n + T_n - M'_p]. \quad (44)$$

Here $M'_p = M_p - \langle \epsilon_R^P \rangle$, and $(M'_n)^2 = M_n^2 + \langle \mathbf{k}_{T-P}^2 \rangle$.

D.3 Comparison to previous analyses

If we set $\mathbf{k}_T^2 = 0$ and $|V_{eff}| = 0$, the above equations are reduced to the equations used in previous analyses except for the fact that the *mean* interaction energies $\langle \epsilon_R^N \rangle$ and $\langle \epsilon_R^P \rangle$ (see Table 3) are used.

E Comparison to ψ' scaling analysis

Maieron, Donnelly, and Sick[13] have done an analysis of higher energy QE *electron scattering* data on nuclear targets within the framework the ψ scaling variable which is defined as:

$$\psi \equiv \frac{1}{\sqrt{\xi_F}} \frac{\lambda - \tau}{\sqrt{(1 + \lambda)\tau + \kappa\sqrt{\tau(1 + \tau)}}}, \quad (45)$$

where $\xi_F \equiv \sqrt{1 + \eta_F^2} - 1$, $\eta_F \equiv K_F/M_n$, $\lambda \equiv \nu/2M_n$, $\kappa \equiv |\mathbf{q}|/2M_n$ and $\tau \equiv |Q^2|/4M_n^2 = \kappa^2 - \lambda^2$.

The ψ' superscaling variable includes a correction that accounts for the removal energy from the nucleus. This

is achieved by replacing ν with $\nu - E_{\text{shift}}$, which forces the maximum of the QE response to occur at $\psi' = 0$. This is equivalent to taking $\lambda \rightarrow \lambda' = \lambda - \lambda_{\text{shift}}$ with $\lambda_{\text{shift}} = E_{\text{shift}}/2M_n$ and correspondingly $\tau \rightarrow \tau' = \kappa^2 - \lambda'^2$ in eq. (45). QE scattering on all nuclei (except for the deuteron) is described using the same universal superscaling function. The only parameters which are specific to each nucleus are the Fermi broadening parameter K_F and the energy shift parameter E_{shift} . The maximum of the QE response is where $\lambda' = \tau'$. This condition yields the following expression for E_{shift}

$$E_{\text{shift}} = \nu_{\text{peak}} + M - M\sqrt{1 + \frac{|\mathbf{q}|^2}{M^2}}. \quad (46)$$

Using the Taylor series expansion $(1 + x)^{1/2} = 1 + x/2 - x^2/8 + x^3/16$ we get for small $|\mathbf{q}|$:

$$E_{\text{shift}} = \nu_{\text{peak}} - \frac{|\mathbf{q}|^2}{2M} + \frac{|\mathbf{q}|^4}{8M^3} - \frac{|\mathbf{q}|^6}{16M^5}. \quad (47)$$

Since $\epsilon_{cc}^P = \nu_{\text{peak}} - \frac{|\mathbf{q}|^2}{2M}$ the expression for E_{shift} becomes:

$$E_{\text{shift}} = \left[\epsilon_{cc}^P + \frac{\nu_{\text{peak}}^2 + (\epsilon_{cc}^P)^2 - 2\epsilon_{cc}^P\nu_{\text{peak}}}{2M} \right] - \frac{(\epsilon_{cc}^P - \nu_{\text{peak}})^3}{2M^2} \quad (48)$$

versus equation 31:

$$\epsilon_R^P = \frac{M_p}{M_p + \nu_{\text{peak}}} \left[\epsilon_{cc}^P + \frac{\nu_{\text{peak}}^2 + (\epsilon_R^P)^2 - \langle (\mathbf{k}_T^P)^2 \rangle}{2M} \right].$$

As shown in Table 3 the values of E_{shift} are similar to the values of ϵ_R^P .

References

1. C. Andreopoulos [GENIE Collaboration], Acta Phys. Polon. B 40, 2461 (2009), C. Andreopoulos (GENIE), Nucl. Instrum. Meth. A614, 87, 2010.
2. H. Gallagher (NEUGEN), Nucl. Phys. Proc. Suppl. 112 (2002).
3. Y. Hayato (NEUT), Nucl. Phys. Proc. Suppl. 112, 171 (2002).
4. D. Casper (NUANCE), Nucl. Phys. Proc. Suppl. 112, 161 (2002). (<http://nuint.ps.uci.edu/nuance/>).
5. J. Sobczyk (NuWro), PoS NUFAC08, 141 (2008); C. Juszczak, Acta Phys. Polon. B40 (2009) 2507. (<http://borg.ift.uni.wroc.pl/nuwro/>).
6. T. Leitner, O. Buss, L. Alvarez-Ruso, U. Mosel (GiBUU), Phys. Rev. C79, 034601 (2009) (arXiv:0812.0587).
7. Omar Benhar, Patrick Huber, Camilo Mariani, Davide Meloni, Physics Reports 700, 1 (2017); Omar Benhar, Donal day, Ingo Sick, Rev. Mod. Phys. 80, 189 (2008); O. Benhar and S. Fantoni and G. Lykasov, Eur Phys. J. A 7 (2000), 3, 415; O. Benhar et al., Phys. Rev. C55. 244 (1997).
8. A. Bodek, M. E. Christy and B. Coppersmith, Eur. Phys. J. C74, 3091 (2014).
9. A. M. Ankowski and J. T. Sobczyk, Phys. Rev. C 74, 054316 (2006).
10. E. J. Moniz, et al., Phys. Rev. Lett. 26, 445 (1971); E. J. Moniz, Phys. Rev. 184, 1154 (1969) ; R. R. Whitney et al. Phys. Rev. C9, 2230 (1974).

11. R. A. Smith and E. J. Moniz, Nucl. Phys B43, 605 (1972).
12. S. Dennis, talk at Nufact 2018, Virginia Tech, Blacksburg, VA; K. Abe, et al., Phys.Rev.Lett. 112, 181801 (2014).
13. C. Maieron, T.W. Donnelly, I. Sick, Phys.Rev. C65 (2002) 025502; J.E. Amaro, M.B. Barbaro, J.A. Caballero, T.W. Donnelly, A. Molinari, and I. Sick, Phys. Rev. C 71, 015501 (2005).
14. P. Gueye et al. Phys. Rev. C60, 044308 (1999).
15. D. Koltun, Phys.Rev.Lett. 28, 182 (1972).
16. O. Hen, G.A. Miller, E. Piasetzky, L.B. Weinstein, Rev. Mod. Phys. 89 (2017) no.4, 045002.
17. A. Bodek and J. L. Ritchie, Phys.Rev. D23, 1070 (1981).
18. Hugh Gallagher, Tufts University, private communication.
19. Jun Chen, Nuclear Data Sheets 140, 1 (2017);
<http://www.tunl.duke.edu/nucldata>;
<http://www.nndc.bnl.gov/nudat2/>.
20. www.periodicTable.com/Isotopes/083.208/index.html;
www-nds.iaea.org/relnsd/vcharthtml/VChartHTML.htm
21. W. M. Seif and Hesham Mansour, Int. J. Mod. Phys. E 24, 1550083 (2015).
22. M. Anghinolfi et, al., J. Phys. G: Nucl. Pan. Phys. 21 (1995) L9-LI5.
23. B. A. Brown, Prog. Part. Nucl. Phys. 47, 517 (2001).
24. *Modern Topics in Electron Scattering*, Edited by B. Frois and I. Sick (World Scientific, Singapore, 1991).
25. D. Dutta et al, (Jlab Hall C), Phys. Rev. C 68, 064603 (2003) ; D. Dutta, PhD Thesis, Northeastern U. (1999).
26. J. Mougey, M. Bernheim, A. Bussire, A. Gillebert, Phan Xuan H, M. Priou, D. Royer, I. Sick, G.J. Wagner, Nucl. Phys A262 (1976) 461; S. Frullani and J. Mougey, Adv. Nucl. Phys. 14, 1(1982).
27. K. Nakamura, S. Hiramatsu, T. Kamae, H. Muramatsu, Y. Watase, Nucl. Phys A268 (1976) 381.
28. K. Nakamura,S. Hiramatsu,T. Kamae,H. Muramatsu, Y. Watas, Nucl. Phys. A296 (1978) 431.
29. K. Nakamura, S. Hiramatsu, T. Kamae, H. Muramatsu, Y. Watase, Nucl. Phys. A271 (1976) 221.
30. G. Jacob and T. A. J. Maria, Rev. Mod. Phys. 43, 6 (1973).
31. N. Liyanage et al, (Jlab Hall A), Phys. Rev. Lett. 86, 5670 (2001); N. Liyanage, PhD Thesis, MIT (1999); K. G. Fissum et al. Phys.Rev. C70, 034606 (2004).
32. P. K. A. de Witt Huberts, J. Phys, G.: Nucl. Part. Phys. (1990) 507; A. E. L. Dieperik and P. K. A. de Witt Huberts, Annu. Rev, Nucl. Part. Sci. 1990. 40:239.
33. G. van der Steenhove et al., Nucl. Phys. A480 547 (1988); ibid A484, 445 (1988).
34. A. M. Ankowski and J. T. Sobczyk, Phys. Rev. C 77, 044311 (2008) (Xiv:0711.2031 [nucl-th]).
35. Vautherin and D. M. Brink, Phys. Rev. C5, 626 (1972).